Biomaterials 178 (2018) 481–495

Contents lists available at ScienceDirect

Biomaterials

journal homepage: www.elsevier.com/locate/biomaterials

Glucocorticoid-loaded liposomes induce a pro-resolution phenotype in human primary macrophages to support chronic wound healing

Anne Gauthier [a, b], Andreas Fisch [a], Klaus Seuwen [c], Birgit Baumgarten [c], Heinz Ruffner [c], Alexandra Aebi [c], Martin Rausch [d], Fabian Kiessling [b], Matthias Bartneck [e], Ralf Weiskirchen [f], Frank Tacke [e], Gert Storm [g, h], Twan Lammers [b, g, h, **], Marie-Gabrielle Ludwig [c, *]

[a] Technical Research and Development, Global Drug Development, Novartis Pharma AG, Basel, Switzerland
[b] Nanomedicines and Theranostics, Institute for Experimental Molecular Imaging, RWTH University HospitalAachen, Aachen, Germany
[c] Chemical Biology and Therapeutics, Novartis Institutes for BioMedical Research, Basel, Switzerland
[d] Biotherapeutic and Analytical Technologies, Novartis Institutes for BioMedical Research, Basel, Switzerland
[e] Department of Medicine III, RWTH University Hospital Aachen, Aachen, Germany
[f] Institute of Molecular Pathobiochemistry, Experimental Gene Therapy and Clinical Chemistry, RWTH University Hospital Aachen, Aachen, Germany
[g] Department of Pharmaceutics, Utrecht University, Utrecht, The Netherlands
[h] Targeted Therapeutics, Biomaterials Science and Technology, University of Twente, Enschede, The Netherlands

ARTICLE INFO

Article history:
Received 6 February 2018
Received in revised form
27 March 2018
Accepted 2 April 2018
Available online 5 April 2018

Keywords:
Liposomes
Glucocorticoid
Macrophage
Targeted delivery
Wound healing

ABSTRACT

Glucocorticoids are well established anti-inflammatory agents, however, their use to treat chronic inflammatory diseases is limited due to a number of serious side effects. For example, long-term local treatment of chronic wounds with glucocorticoids is prohibited by dysregulation of keratinocyte and fibroblast function, leading to skin thinning. Here, we developed and tested liposome formulations for local delivery of dexamethasone to primary human macrophages, to drive an anti-inflammatory/pro-resolution phenotype appropriate for tissue repair. The liposomes were loaded with the pro-drug dexamethasone-phosphate and surface-modified with either polyethylene glycol or phosphatidylserine. The latter was used to mimic phosphatidylserine-harboring apoptotic cells, which are substrates for efferocytosis, an essential pro-resolution function. Both formulations induced a dexamethasone-like gene expression signature in macrophages, decreased IL6 and TNFα release, increased secretion of thrombospondin 1 and increased efferocytosis activity. Phosphatidylserine-modified liposomes exhibited a faster uptake, a higher potency and a more robust phenotype induction than polyethylene glycol-modified liposomes. Fibroblast and keratinocyte cell cultures as well as a 3D skin equivalent model showed that liposomes applied locally to wounds are preferentially phagocytosed by macrophages. These findings indicate that liposomes, in particular upon shell modification with phosphatidylserine, promote dexamethasone delivery to macrophages and induce a phenotype suitable to support chronic wound healing.

1. Introduction

Chronic inflammatory diseases such as rheumatoid arthritis, atherosclerosis, chronic obstructive lung disease (COPD), autoimmune diseases and chronic skin wounds still represent a major unmet medical need. To a large extent, the inflammatory state is regulated by the innate immune system, with macrophages playing a central role [1]. Chronic inflammatory conditions are characterized by a constant influx of monocytes, a sustained high number of active pro-inflammatory macrophages, combined with a relative lack of anti-inflammatory/pro-resolution macrophages that actively support the resolution of inflammation and promote tissue repair [2–4].

In the skin, chronic wounds are generally characterized as open

* Corresponding author.
** Corresponding author. Nanomedicines and Theranostics, Institute for Experimental Molecular Imaging, RWTH University HospitalAachen, Aachen, Germany.
E-mail addresses: tlammers@ukaachen.de (T. Lammers), marie-gabrielle.ludwig@novartis.com (M.-G. Ludwig).

https://doi.org/10.1016/j.biomaterials.2018.04.006
0142-9612/

wounds in a chronic inflammatory state [5–9], with an important bacterial colonization, leukocyte entrapment and prolonged pro-inflammatory mediator secretion, including TNFα, IL6 and IL1β [10–12]. This pro-inflammatory environment induces macrophage phenotypes with deficient phagocytic activity resulting in the build-up of necrotic debris. Wound fluid also contains high levels of proteases such as matrix metalloproteinases (MMPs) and low levels of tissue inhibitor of metalloproteinases (TIMPs), due to the sustained presence of neutrophils [13,14], which favors extracellular matrix degradation [7]. In such environments keratinocytes and fibroblasts tend to become senescent, and their migration and proliferation capacities are impaired [15,16]. This leads overall to a persistent inflammatory state that prevents resolution and tissue repair.

Glucocorticoids (GCs) are highly potent, clinically routinely used anti-inflammatory agents acting on macrophages via complex mechanisms of direct and indirect transrepression or transactivation of gene expression mediated by the GC receptor (GR) [17]. The GC-induced phenotype not only exhibits a decrease in inflammatory activities, but also the induction of processes involved in the resolution of inflammation and wound healing. The anti-inflammatory action of GCs is mediated by interfering with specific signaling pathways, including a reduced production of pro-inflammatory cytokines such as IL6 or TNFα. On the other hand, a number of genes positively regulated by the GR contribute to the pro-resolution and regenerative activity of macrophages [18].

Efferocytosis, the removal of apoptotic neutrophils before they undergo secondary necrosis, is a critical macrophage activity limiting tissue damage and supporting recovery [19,20]. GCs stimulate efferocytosis by upregulating the membrane receptor MerTK which is involved in the recognition of the phospholipid phosphatidylserine (PS) exposed on apoptotic cells [21–23]. Of note, the process of phagocytosing apoptotic cells itself contributes to the anti-inflammatory function of macrophages by inducing TGFβ1 and IL10 release [24–27] and by suppressing pro-inflammatory cytokine production [19,23,24,26,28]. Hence, GC-induced macrophage polarization and efferocytosis generate a positive feedback loop for resolution.

However, as GRs are expressed in most cell types and since GCs have a large volume of distribution, treatments with GCs lead to side effects that limit their use in systemic applications, in particular for long term treatments at high doses. In the context of skin wounds, skin atrophy and impaired healing are typical side effects of both systemic and topical GC therapies [29–32]. Skin atrophy is characterized by thinning of the epidermal layer (decreased keratinocyte numbers), loss of elasticity, increased permeability (disrupted skin barrier function), dermal atrophy due to low number of fibroblasts and decreased levels of extracellular matrix (e.g. collagen, hyaluronan proteins) [32–34]. Strategies to overcome these limitations include the use of nanomedicine formulations, such as liposomes, to improve cell-specific delivery and sustain on-site drug availability.

In this study, we set out to compare two formulations, based on liposomes containing in their lipid bilayer either 10% PS or polyethylene glycol (PEG) exposed at the surface. GCs were encapsulated in both formulations in the form of the pro-drug dexamethasone phosphate (DexP), which is known to be processed in phagocyte lysosomes to deliver active dexamethasone (Dex) into the cell cytoplasm. PS-containing liposomes may be able to mimic PS-harboring apoptotic cells and their resolution enhancing properties. We first evaluated these formulations *in vitro* with regards to efficacy of delivery, and their ability to induce an anti-inflammatory state and pro-resolution functions. In a second step we evaluated the targeting of liposome-mediated dexamethasone delivery to macrophages, as compared to liposome uptake by keratinocytes and fibroblasts, in 2D cultures and in a 3D skin equivalent model. The preferential liposome uptake by macrophages suggests that local delivery of GCs specifically to monocytes/macrophages via liposomes represents a new therapeutic avenue for the treatment of chronic wounds.

2. Materials and methods

2.1. Liposome preparation and characterization

Dipalmitoylphosphatidyl choline (DPPC), PEG-(2000)-distearoylphosphatidyl ethanolamine (PEG-(2000)-DSPE) and Dioleylphophatidyl serine sodium salt (DOPS) were obtained from Lipoid (Steinhausen, Switzerland) and Cholesterol HP was obtained from Dishman (Veenendaal, Netherlands). All chemicals were of reagent grade. Liposome formulations were prepared with the film method. For PEG liposomes, DPPC, cholesterol and PEG-(2000)-DSPE were mixed at a molar ratio of 1.85:0.15:1 and dissolved in ethanol. For PS liposomes, DPPC, cholesterol and DOPS were mixed at a molar ratio of 1.7:0.3:1 (equivalent to 10 mol% DOPS relative to the total lipid amount) and dissolved in ethanol. The final lipid concentration was 100 mM for both formulations. The organic phase was evaporated with a rotavapor (BUCHI Labortechnik, Flawil, Switzerland) until a lipid film was obtained. Residual organic solvent was removed by placing the films overnight on a tabletop lyophilisator (Christ Alpha1-2 LD, Martin Christ Gefriertrocknungsanlagen, Osterode am Harz, Germany). For dexamethasone 21-phosphate disodium salt (DexP) (Sigma-Aldrich, Buchs, Switzerland) loaded liposomes, the lipid films were hydrated at 50 °C with a 50 mg/mL DexP aqueous dextrose solution (Hospira, Lake Forest IL, USA). Drug-free formulations where hydrated with 5% dextrose. The liposomes were extruded at 50 °C (Lipex, Northern Lipids, Vancouver, Canada) under nitrogen pressure through Whatman polycarbonate membranes with a pore size of 1 μm and then 100 nm (GE Healthcare, Glattburg, Switzerland). Non-encapsulated DexP was removed by dialysis at 4 °C against 5% dextrose using a Float-a-Lyzer G2 (Sigma-Aldrich) with a cut-off of 100 kDa. Liposomes were diluted 1:100 in sterile-filtered phosphate-buffered saline (PBS) pH 7.4 (Sigma-Aldrich) before use *in vitro*. DexP liposomes were prepared freshly every second week. Fluorescent drug-free DiD and DiI liposomes were prepared as the other formulations, with an additional 1 mol% of DiD or DiI (Biotium, Fremont CA, USA) relative to the total lipid concentration added to the lipid mix in ethanol.

The mean particle size, polydispersity index (PDI) and zeta potential were measured using a Malvern Zetasizer Nano ZS (Malvern Instruments, Malvern, UK) (Supplement Fig. 1). Target size for liposomes was between 100 and 150 nm. Expected zeta potential values are close to neutral for PEGylated liposomes and negative for PS-containing liposomes.

The DexP amount retained inside the liposomes was determined by High Performance Liquid Chromatography (HPLC) (1100 Series, Agilent Technologies, Basel, Switzerland) using a mobile phase of acetonitrile and water (35:65) at pH 2 (pH adjustment with 0.1% v/v phosphoric acid). Eluents were measured with a UV-detector at 242 nm, passing through a ZORBAX SB-C18 column 1.8 μm; 4.6 × 100 mm (Agilent Technologies).

For assessing the cytotoxicity of liposomes, monocytes were seeded in 96-well plates at 2×10^5 cells per well and treated as described for 24 h. The assay was performed immediately, following the manufacturer's protocol (Cayman Chemicals, Hamburg, Germany). The absorbance of the solution (dissolved formazan crystals) was measured at 570 nm on a SpectraMax 340 microplate reader (Molecular Devices, Sunnyvale CA, USA) and reported as a percentage of viability/metabolism relative to the

control.

2.2. In vitro cell culture

Primary cells were sourced and handled in a BL2 safety environment according to the Swiss legislation. Buffy coats (Blood Center, Bern, Switzerland) were from anonymized donor source.

Standard cell treatments include dexamethasone (Dex) (ABCR GBMH, Karlsruhe, Germany) at a concentration of 1 μg/mL (2.5 μM). DexP is a pro-drug not able to efficiently cross lipid bilayers and therefore retained in the aqueous core liposomes; upon phagocytosis of the liposome, DexP is efficiently cleaved in the endosomes/lysosomes to the active form Dex which can partition into the cytosol or the nucleus where it exerts its transcriptional effects. Hence, DexP-loaded liposomes were used at a nominal concentration equivalent to 1 μg/mL DexP (referred to as PEG or PS DexP liposome treatments). For other free Dex concentrations, the DexP-loaded liposome concentrations were similarly adjusted. Equivalent amounts of drug-free PEG or PS liposomes were added accordingly; untreated cells are referred to as controls. In experiments using fluorescent DiD- or DiI-labeled liposomes, these were added in amounts equivalent to those used in drug-free liposome experiments.

Primary human monocytes were isolated as described in Ref. [35]. Essentially, peripheral blood mononuclear cells (PBMCs) from healthy blood donors were purified by Ficoll density gradient centrifugation. Monocytes were then isolated by magnetic sorting using a human CD14 negative selection kit (Easysep, Stemcell Technologies, Köln, Germany) according to the manufacturer's instructions and frozen at −80 °C until use. The purity of isolated monocytes, assessed by CD14 flow cytometry, was in the range of 80–95%.

For culture, monocytes were quickly thawed and resuspended in IMDM (Thermo Fisher Scientific, Reinach, Switzerland) supplemented with 10% HS, 1× non-essential amino acids (Thermo Fisher Scientific), 2 mM Glutamax (Thermo Fisher Scientific), 1 mM Na-pyruvate (Thermo Fisher Scientific), 4 μg/mL human insulin (Thermo Fisher Scientific), 5 ng/mL human recombinant M-CSF (R&D Systems, Minneapollis MN, USA) and 1% Penicillin/Streptomycin (Pen/Strep) (BioConcept, Allschwill, Switzerland) for culture at 37 °C with 5% CO_2. Monocytes were plated, immediately treated and macrophages were cultured for 24 h, unless otherwise stated. Pro-inflammatory mature macrophages were generated by culture for 3 days in the presence of INFγ (R&D Systems) at 10 ng/mL.

Human primary dermal keratinocytes (CellnTec, Bern, Switzerland) were cultured in CnT-Prime epithelial culture medium (CellnTec); cell passages of 4 or 8 were used in the experiments.

Human primary dermal fibroblasts (ATCC, Manassas VA, USA) were grown in DMEM/HAM F12 (1:1) supplemented with 10% fetal calf serum (FCS) (BioConcept) and 1% pen/strep, at 37 °C, 5% CO_2. Cells were detached with trypsin and split as required for assays.

2.3. Expression profiling

Monocytes were seeded in 12-well culture plates (TPP, Sigma-Aldrich) at 1×10^6 cells per well. After treatment, cells were lysed in trizol (Molecular Research Center, Cinicinnati OH, USA) and RNA was purified using the Direct-zol™ RNA Miniprep kit (Zymo Research, Freiburg im Brisgau, Germany) following the manufacturer's instructions, including the DNase digestion step (RNase-Free DNase Set, Qiagen). Reverse transcription was performed using the SuperScript® III First-Strand Synthesis System (Thermo Fisher Scientific) according to the manufacturer's instructions. Briefly, primers (oligodT20 2.5 μM, dN6 2.5 ng/μL) and dNTPs (0.5 mM) were added to 0.2–1 μg RNA, incubated for 5 min at 65 °C, then on ice for 1 min. The cDNA synthesis mix (RT buffer 1×, RNase inhibitor, 10 mM DTT, 5 mM $MgCl_2$, reverse transcriptase) was added and incubated for 10 min at 25 °C, 50 min at 50 °C and 5 min at 85 °C, followed by RNase H treatment for 20 min at 37 °C. Quantitative polymerase chain reaction (qPCR) was performed following the manufacturer's protocol and using TaqMan probes (Thermo Fisher Scientific) (Supplement Table 1). The reaction mix contained 5 μL Universal PCR Master Mix (Thermo Fisher Scientific), 0.5 μL probe (20× concentrated), 2 μL cDNA (2.5 ng/μL) and 2.5 μL water. The reaction was run in 384-well MicroAmp Optical reaction plates (Thermo Fischer Scientific). Microfluidic cards (custom-made array, Thermo Fisher Scientific) (Supplement Table 1) were used according to the manufacturer's instructions, with 50 μL of cDNA (150 ng/mL) per lane. The assays were run using the 7900HT Fast Real-Time PCR System or the QuantStudio 7 Flex PCR system (Thermo Fisher Scientific) with the following cycling conditions: 50 °C for 2 min, 95 °C for 10 min, 40 cycles at 95 °C for 15 s and 60 °C for 1 min. Data analysis was done using the $2^{-\Delta\Delta Ct}$ method and reported as HPRT normalized expression levels or as fold change compared to control.

2.4. Flow cytometry

Monocytes were seeded in thermo-sensitive Nunc UpCell 48-well plates (VWR, Dietikon, Switzerland) at 5×10^5 cells per well (2 wells/antibody). After treatment, plates were put on ice for 15 min for cell detachment and then distributed in a 96-well plate (Sigma-Aldrich) at 3×10^5 cells per well and incubated 15 min in blocking buffer (1 mM EDTA, 20% HS in PBS) on ice, in the dark. MerTK and CD163 primary antibodies and isotype control (MAB8912, MAB1607 and MAB002, R&D Systems) were added for 1 h, before washing and further incubation with the secondary antibody for 30 min (A21200, Thermo Fisher Scientific). After fixation with 1% PFA, cells were resuspended in 300 μL PBS for immediate analysis. Flow cytometry experiments were read on a CyAn ADM (Beckman Coulter, Nyon, Switzerland) or a FACSCanto II (BD Biosciences). Data analysis was performed with the FlowJo software 7.6.5 (BD Biosciences).

2.5. IL6 and TNFα cytokine release assays

Monocytes were seeded in 96-well plates (Sigma-Aldrich) at 2×10^5 cells per well and treated immediately or previously differentiated to control or pro-inflammatory mature macrophages as described in specific experiments. 10 ng/mL LPS (Sigma-Aldrich) was added for the last overnight and supernatants were stored at −80 °C until use. IL6 and TNFα were measured using Homogeneous Time-Resolved Fluorescence (HTRF)-based assays (Cisbio Bioassays, Codolet, France) and according to the manufacturer's instructions. Supernatants for IL6 analysis were diluted 1:5 and supernatants for TNFα measurement were diluted 1:10 prior to performing the assay. The donor fluorophore emission at 620 nm and the acceptor fluorophore emission at 665 nm were read on an EnVision 2104 Multilable plate reader (PerkinElmer, Schwerzenbach, Switzerland).

2.6. Thrombopsondin1 release

Monocytes were seeded in 24-well plates (TPP) at 6×10^5 cells per well and treated as described. Supernatants were collected and stored at −80 °C until use. Thrombopsondin1 (TSP1) was measured in cell culture supernatants, diluted 1:5, using an enzyme-linked immunoassay (ELISA), following the manufacturer's instructions (R&D Systems). The optical density was measured on a SpectraMax 340 microplate reader (Molecular Devices) at 450 nm.

2.7. Efferocytosis assay

Monocytes were plated in a 96-well plate (Ibidi, Vitaris, Baar, Switzerland) at 1.2×10^5 cells per well and labeled simultaneously with 2.5 μM of CellTracker™ Green CMFDA (5-chloromethylfluorescein diacetate, Thermo Fisher Scientific). The cells were then treated as described daily for 3 days before assessment of the efferocytosis capacity of the mature macrophages.

Jurkat A3 cells (Acute T cell leukemia, ATCC) were cultured in RPMI 1640 supplemented with Glutamax (Thermo Fisher Scientific) and 10% FCS. On the day prior to the experiment, cells were seeded in a 48-well plate (Thermo Fisher Scientific) at 1×10^6 cells per well and induced to apoptosis by addition of 10 ng/mL FAS activating antibody (Merck, Zug, Switzerland) in serum-free medium overnight. On the day of experimentation, the Jurkat apoptosis rate was evaluated on a cell culture aliquot by staining with Annexin V-AlexaFluor®488 (Thermo Fisher Scientific) at 1:50 and a viability dye (Fixable Viability Dye eFluor® 660, Thermo Fisher Scientific) at 1:500 in buffer (10 mM HEPES, 140 mM NaCl, 2.5 mM $CaCl_2$, pH7.4). After 15 min incubation at room temperature in the dark, the cells were washed twice and analyzed by flow cytometry. After ensuring an apoptosis rate of at least 70% and less than 5% cells having undergone secondary necrosis, cells were stained for 30 min with Cell Trace™ Violet (Thermo Fisher Scientific) 1:1000 in PBS, washed 3 times with PBS and resuspended in culture medium.

Efferocytosis was initiated by adding Cell Trace™ Violet-stained apoptotic Jurkat A3 cells on the day 3 treated-macrophages at a 3:1 ratio and incubated for 60 min at 37 °C, 5% CO_2. The wells were then washed twice to remove excess Jurkat A3 cells and fixed with 1% PFA before evaluation of the phagocytosis by imaging using an Operetta® high content screening system (PerkinElmer). Analysis was performed with the Harmony 4.1 software (PerkinElmer) and an embedded algorithm that allows for the identification of cells and as well as the differentiation of the two cell populations used (green channel for macrophages and blue channel for Jurkat cells). The efferocytosis rate was determined by counting the number of green objects with blue overlaps (Jurkat in macrophages) over the total number of green objects (macrophages). 15 fields were acquired per well for this calculation and each condition was plated in triplicate.

2.8. Confocal microscopy

Macrophages were seeded in an 8-well μ-slide (Ibidi) at 1.5×10^5 cells per well and left to attach for 24 h. On the day of the experiment, cells were stained with CellTracker Green CMFDA (5 μM) for 30 min, and treated with DiD liposomes for the indicated time points. At each time point, cells were washed with PBS and fixed with 1% PFA. Slides were stored at 4 °C until imaging. To show the active uptake of liposomes, 5 μg/mL of Cytochalasin D (Sigma-Aldrich) was pre-incubated for 30 min with the cells before addition of DiD liposomes.

Keratinocytes and fibroblasts were plated at 5×10^4 cells per well and 1.5×10^4 cells per well, respectively, and incubated 24 h before staining with CMFDA, treatment with DiD liposomes for 24 h, and analyzed as described above.

Confocal images were captured at 488 and 639 nm excitation wavelength using a Zeiss LSM710 inverted microscope (Carl Zeiss, Feldbach, Switzerland). For quantification, images of 4 randomly selected regions per well were taken. The fluorescence of the green macrophages and of the red liposomes was quantified by calculating the respective surface areas using the ImageJ software (NIH, USA).

2.9. 3D full thickness skin model

In order to generate the dermin of the 3D skin model, human primary dermal fibroblasts (PromoCell, Heidelberg, Germany) were expanded in DMEM and HAM F12 (1:1) with Glutamax (Thermo Fisher Scientific) and 10% FBS (Thermo Fisher Scientific). The RAFT kit (Lonza, Visp, Switzerland) enabled the creation of a cell-collagen solution according to the manufacturer's instructions. Briefly, a 24-well 6.5 mm Transwell plate with 0.4 μm Pore Polyester Membrane single inserts (Sigma-Aldrich) was seeded with the cell-collagen solution at a density of 4×10^4 cells per well, in medium containing 5% FBS and freshly supplemented with 284 μM L-Ascorbic acid (Sigma-Aldrich); absorbers were added for 15 min to condense the cell-collagen mix. The cells were left to mature for 1 week at 37 °C, 5% CO_2 and medium was changed every 2–3 days.

For the epidermis, human primary dermal keratinocytes (CellnTec) were expanded in CnT-PR medium (CellNTec). For the seeding of the keratinocytes into the construct, medium from the fibroblasts was removed from the inserts and the wells. Silicone plugs (Oris Cell Migration Assay Kit-96-well plates with Oris Cell Seeding Stoppers, Platypus Technologies, Madison WI, USA) were placed for the creation of wounds on top of the fibroblast-collagen dermis in inserts. Keratinocytes were added at a density of 2×10^5 cells per insert on the top of the collagen-fibroblast matrix around the stopper. KBM medium supplemented with KGF, 0.15 mM Ca^{2+} (Lonza) was added into the inserts and into the wells, and models were incubated for 2 days whereby keratinocytes were covered with medium. To equilibrate the epidermal equivalent for stratification, medium in the inserts and the wells was replaced by KBM medium supplemented with KGF, 1.3 mM Ca^{2+}, 10 μg/mL transferrin (Thermo Fisher Scientific), 0.1% BSA (Sigma-Aldrich) and 50 μg/mL L-ascorbic acid (Lonza) before models were incubated overnight, whereby keratinocytes were covered with medium. To start the keratinocyte stratification process at the air-liquid interface (ALI), medium was removed the next day, and fresh medium was re-applied only to the wells but not to the insert so that the medium level in the former just reached the bottom of the filter insert, leaving the keratinocyte layer exposed to air. The model was kept under ALI conditions for 6 days with a medium change every 2–3 days.

On the day of assay start, the silicone plug was removed and DiI fluorescent liposomes, alone or along with 1.8×10^4 CMFDA-stained day 1 macrophages, were added into the wound. After 24 h incubation, the skin model was cut out from the insert with a scalpel and laid flat in an optically clear bottom 24-well μ-plate (Ibidi) for imaging. In a parallel setting, with sole addition of liposomes into the wound, the skin construct was stained for 1 h with 2 μM Calcein green (Thermo Fisher Scientific) before imaging, to allow for better identification of keratinocytes and fibroblasts.

Images were taken on an inverted two-photon (2P) excitation laser scanning microscope (FVMPE-RS Laser Scanning Microscope, Olympus Volketswil, Switzerland) using a water-immersed 25×, NA1.0 lens (Olympus). For 2P excitation a Spectra-Physics DS + laser (Munich, Germany) was used to provide two simultaneous pulsed laser outputs, one variable output ranging from 690 to 1300 nm and one fixed output at 1024 nm. The excitation wavelength was set to 800 nm to excite CMFDA cell tracker green or calcein green and 1024 nm for excitation of DiI. Liposomes appeared in red and cells from the model (macrophages or keratinocytes and fibroblasts) appeared in green. Images were taken in selected areas and z-stacks were performed over the zone of interest around the wound, covering a range of approximately 100 μm in axial direction with 2 μm distance between the images.

2.10. Statistical analysis

Statistical analysis was performed with GraphPad Prism 7 (Graphpad Software, La Jolla, CA, USA) using the appropriate statistical tests as indicated in the figure legends. A value of $P < 0.05$ was considered as statistically significant: $^{*}P < 0.05$; $^{**}P < 0.001$.

3. Results and discussion

3.1. Establishment of the delivery platform

Stealth liposomes containing surface-exposed PEG in their membrane (PEG liposomes) have been developed as one of the most promising liposome-based delivery systems [36]. Their utility for treatment of inflammatory diseases has been shown in preclinical models as well as in clinical trials [37–41]. We used this formulation as reference and compared its functionalities to liposomes containing 10% PS in their membrane (PS liposomes). The use of PS in liposome formulations has already been investigated, mainly for the negative charge it induces at the membrane, favoring uptake by phagocytes. However, the PS exposed on the membrane of apoptotic cells is also known to exhibit biological functions that we aim at exploiting [42]. In the liposome membranes, it may mimic the 'eat me' anti-inflammatory signals sent to macrophages upon recognition [43]. In the macrophages, this may *per se* induce anti-inflammatory responses that could synergize with the effects related to concomitant Dex delivery to the cells.

Liposome preparation and DexP loading were performed following the well-established lipid film hydration method. All formulation preparations were characterized for their physical properties and DexP loading, and the absence of toxicity on macrophages was verified (Fig. 1 and Supplement Fig. 1). Preparations for PEG and PS liposomes were comparable with regard to size (100–150 nm) and PDI (lower than 0.2). The homogenous size distribution for each DexP formulation was confirmed by size distribution profiles (Supplement Fig. 1). As expected, the zeta potential of the PEG liposomes was close to neutral and negative for the PS liposomes. HPLC-quantified DexP concentrations indicate that approximately 5 mg/mL DexP was encapsulated regardless of the lipid composition.

For routine experiments, free Dex or DexP in liposomes was used at 1 μg/mL which is in the range of published studies. At this concentration free Dex exerts a close to maximal transcriptional effect on macrophages [35,44] and the required liposome concentration is non-toxic ([45] and Fig. 1).

3.2. PEG and PS DexP liposomes induce an inflammation-suppressing gene signature and are rapidly taken up by macrophages

Macrophages were stimulated with free Dex or liposomes loaded with DexP (DexP liposomes) for 24 h. It is known that free Dex can induce a gene expression signature within this time frame (microarray study deposited at ArrayExpress, E-MTAB-5913). Also, this short treatment time will allow for a detailed study of the kinetics of liposome uptake and its translation into effective Dex activity in the macrophages. We selected a Dex-specific gene signature based on markers linked to anti-inflammatory or pro-resolution roles: ALOX15B (synthesis of pro-resolving lipoxins), CD163 (hemoglobin/haptoglobin complex-binding scavenger receptor; heme uptake), IL1R2 (decoy receptor for IL1α, IL1β, IL1RA), MERTK (efferocytosis receptor) and SEPP1 (major selenium transporter; extracellular antioxidant). Hence this signature corresponds to an inflammation-suppressing and resolution-promoting macrophage phenotype. The expression of several other genes, modulated by other macrophage polarizing agents, was measured to evaluate the specificity of the liposome-induced effects.

Using macrophages derived from two donors, we confirmed the upregulation of the Dex signature by free Dex and showed that it was similarly achieved with DexP liposomes (Fig. 2). The fold changes of mRNA expression levels were in the same range as those observed for free Dex for all genes measured. Only few of the IL4 or IFNγ signature genes responded and changes were moderate compared to genuine IL4 or IFNγ stimulation (see Fig. 6A for CD38 upregulation by IFNγ or our microarray data (E-MTAB-5913) for all listed genes). This assay confirms the functional uptake of DexP liposomes by macrophages, including DexP hydrolysis to release intracellular Dex, and validates our delivery platform. Using this gene expression readout, both DexP liposome formulations exhibited similar efficacies at 24 h post-treatment. It should be noted that the liposomes themselves exhibited a very limited effect on the macrophage transcriptome; this shows the specificity of the macrophage response to the DexP formulations and demonstrates the absence of liposome-induced cytotoxicity. Furthermore, donor variability in macrophage responses is similar for DexP liposomes and free Dex, highlighting the consistent behavior of the DexP liposomes as compared to free Dex treatments.

In order to better characterize the behavior of the two formulations in their interaction with macrophages, we performed kinetic studies. We prepared drug-free PEG and PS liposomes labeled with DiD in their membrane to allow for tracking by microscopic imaging. Physical properties of the liposomes were verified (Supplement Fig. 1) and were found similar to those of the non-labeled liposomes. Confocal microscopy images of CMFDA-labeled macrophages (green) and red DiD liposomes co-incubated for 1 h, 4 h, 6 h or 24 h were taken (Supplement Fig. 2). Quantification of the liposome uptake suggested a progressive phagocytosis by macrophages, with, as hypothesized, a faster kinetics for the PS liposomes for which overlapping green and red signals are already measurable after 4 h of incubation (Fig. 3A). At 24 h, both formulations appear phagocytosed within macrophages, in good agreement with the expression profiling data at this time point, PS liposomes showing a better uptake than PEG liposomes in this experiment. Internalization of PEG and PS liposomes within macrophages is shown in a z-stack visualization (Fig. 3B). Treatment of macrophages with cytochalasin D completely blocked liposome uptake, showing that it is an active process, as it is for apoptotic cells (Fig. 3C). These results correlate with an effective delivery of Dex to macrophages relying on DexP liposome internalization.

We next measured the consequence of liposome uptake at the functional level, using qPCR expression profiling. Expression of a gene panel selected from the Dex signature was followed over time, until 24 h. Different kinetic profiles are seen for individual genes with free Dex, and overall well reproduced with the DexP liposomes, with similar mRNA levels observed at 24 h for the free Dex and DexP liposome conditions (Fig. 4A). Between the two formulations, PS DexP liposomes exhibit a slightly faster and higher increase in gene transcription at short time points as compared to PEG DexP liposomes. This is in good agreement with the faster uptake of PS liposomes seen previously (Fig. 3A). It is noticeable that MERTK induction is delayed, its mRNA starting to increase only at the 24 h time point, which is in line with the known indirect modulation of MERTK expression by GCs. To the contrary, for example, CD163 is directly activated by the GR and a GR response element (GRE) is found in its promoter region [46].

We analyzed how this transcription kinetics relates to the protein levels that are required for functionality. We compared membrane expression of CD163 and MerTK, at different treatment times: (i) 24 h, or (ii) 3 days with treatment for the first 24 h followed by washing, or (iii) daily for 3 days (Fig. 4B). Upregulation of

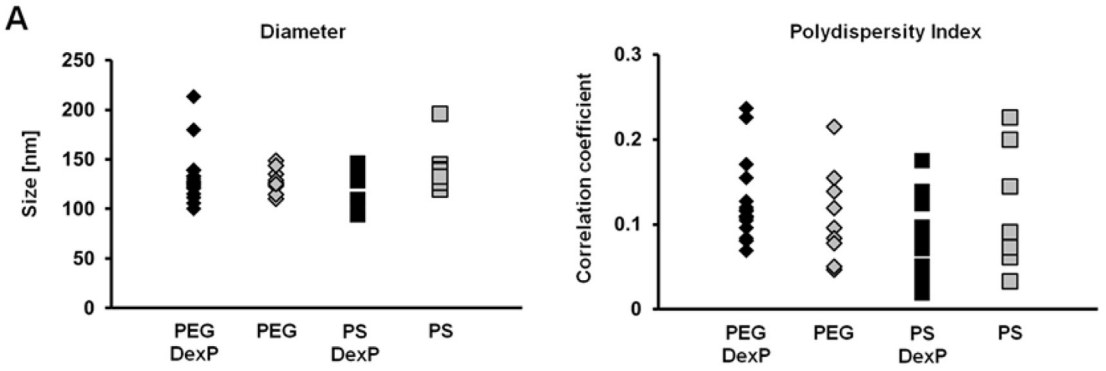

B

Formulations	Zeta Potential
	mV
PEG DexP	-0.81 ± 0.66
PEG	0.08 ± 1.08
PS DexP	-15.25 ± 2.87
PS	-14.67 ± 5.28

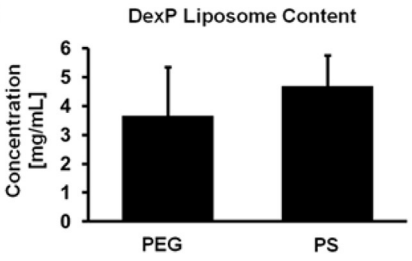

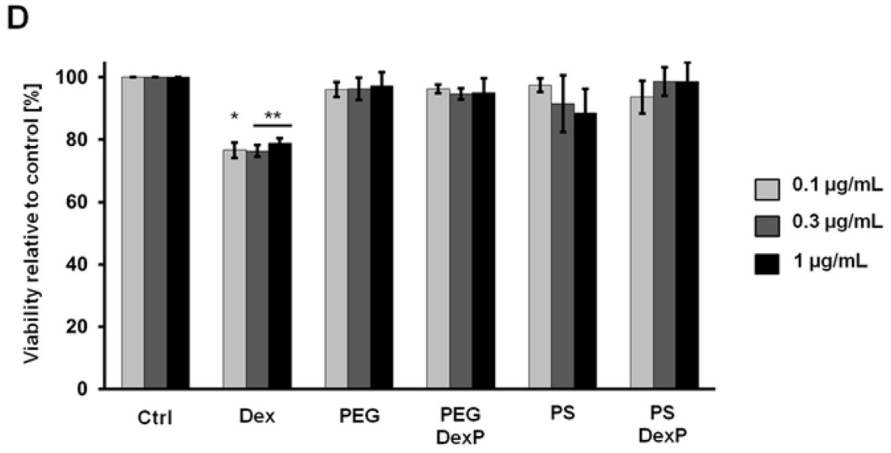

Fig. 1. Characterization of PEG and PS liposome preparations. PEG and PS liposomes were manufactured using the lipid film hydration method. The formulations were hydrated with 50 mg/mL DexP in dextrose or with dextrose alone for the controls. The values of 18 preparations for the DexP formulations and 10 preparations for the control formulations are shown. (A) Size and PDI were measured by dynamic light scattering. (B) Zeta potential was measured by electrophoretic mobility; average values are indicated. (C) DexP average concentration was measured by HPLC and is displayed as mg of DexP per mL of liposome suspension; error bars represent the SD for all 18 preparations. (D) Primary human monocytes were treated for 24 h with free Dex or DexP liposomes at a nominal Dex concentration of 0.1–0.3-1 µg/mL. Metabolic activity/viability was assessed using an MTT assay and is shown relative to untreated cells (Ctrl) for three independent experiments in technical triplicates (error bars represent the SD). A one-way ANOVA followed by Tukey's multiple comparisons test compare free Dex and DexP liposome treatments to control cells with $^{*}P < 0.05$ and $^{**}P < 0.001$.

CD163 was observed already at 24 h of treatment, for free Dex and PS DexP liposomes, and was similar in the other treatment settings, suggesting that maximal induction had been reached. Interestingly, the transient higher CD163 mRNA levels observed with free Dex compared to DexP PS liposomes in the kinetic study (Fig. 4A) did not translate at the protein level after 24 h of treatment. PEG DexP liposomes induced a minor upregulation of CD163, suggesting a lower efficacy of this formulation. MerTK exhibited a delayed increase in membrane expression, as expected from the transcription kinetics, and was maximally upregulated after 3 days of treatment. DexP PS liposomes induced MerTK at levels similar to those observed in free Dex treated macrophages. Using membrane receptor levels as readout, PEG liposomes exhibited less robust effects, confirming the higher efficacy of PS liposomes for Dex delivery to macrophages. Drug-free liposomes had no effect on transcription of these genes in the investigated time frame (Figs. 3A and 7E and Supplement Fig. 2).

3.3. Characterization of the anti-inflammatory/pro-resolution microenvironment induced by DexP liposomes-treated macrophages

Next we measured the capacity of DexP liposome-treated macrophages to modulate pro- and anti-inflammatory factor release. Free Dex potently reduced LPS-induced TNFα and IL6 release, as expected. The measured IC50s of 3.1 ng/mL for TNFα and 9.9 ng/mL for IL6 are in the range of values previously published [35]. Both DexP liposome formulations decreased the release of the pro-inflammatory cytokines, but at lower potency than free Dex (Fig. 5A). For TNFα, for which the inhibitory effect was stronger than for IL6, the DexP liposome IC50s were roughly 100 times higher

GENES	Type	Dex	PEG DexP	PS DexP	PEG	PS	Dex	PEG DexP	PS DexP	PEG	PS
		Donor 1					Donor 2				
HPRT1		1.00	1.00	1.00	1.00	1.00	1.00	1.00	1.00	1.00	1.00
ALOX15B	Dex	37.92	30.02	23.09	9.08	1.48	193.08	124.36	93.42	33.95	4.42
CD163	Dex	5.02	5.18	3.76	2.43	1.13	3.97	4.08	4.38	1.64	0.95
IL1R2	Dex	11.50	11.84	4.16	2.38	0.45	20.64	19.06	21.69	1.64	1.78
MERTK	Dex	2.22	2.62	2.09	1.24	0.95	2.05	2.50	2.96	0.93	0.81
SEPP1	Dex	14.17	9.43	11.16	3.61	3.68	12.83	14.88	10.62	10.74	2.52
CLEC10A	IL4	2.49	2.81	2.93	1.93	0.92	2.82	3.18	5.56	2.53	1.33
CCL13	IL4	0.30	0.60	0.44	1.54	0.24	0.40	0.54	1.12	0.57	0.52
CCL18	IL4	1.79	2.51	8.21	2.33	6.11	0.47	0.53	1.74	0.93	1.29
CCL23	IL4	0.69	0.70	4.83	0.70	2.68	0.35	0.45	0.95	0.65	0.94
GPX3	IL4	0.31	0.32	0.38	0.41	0.88	0.58	0.40	1.26	1.60	1.91
MAOA	IL4	0.44	0.45	0.17	0.86	0.16	1.02	0.93	1.42	0.68	0.97
TREM2	IL4	0.27	0.28	0.20	0.84	0.59	0.66	0.59	0.74	1.69	1.74
FCGR2A	IL4	1.78	1.65	1.21	1.48	0.63	1.73	1.61	1.70	0.76	0.71
FCGR2B	IL4	1.31	1.43	5.55	0.92	0.57	2.94	2.31	11.42	2.00	0.98
CD14	IL4	1.10	1.02	2.27	0.85	1.54	1.09	1.25	2.68	1.18	1.06
CD38	IFNγ	9.07	7.03	4.36	2.53	0.44	3.12	4.33	8.02	1.66	0.59
CXCL10	IFNγ	0.43	0.73	0.26	1.54	0.04	0.10	0.06	0.76	0.30	0.07
CXCL11	IFNγ	0.46	0.34	0.35	1.07	0.05	0.11	0.10	0.61	0.09	0.11
CXCL9	IFNγ	0.79	0.79	1.20	1.89	0.93	0.25	0.18	0.39	1.32	0.40
TNF	IFNγ	0.65	0.63	0.54	0.73	0.53	1.05	0.69	1.61	1.31	0.97
TNFAIP6	IFNγ	1.06	1.39	2.32	0.97	0.57	0.99	0.70	3.16	0.77	0.63

> 2 > 5 > 10 > 50

Fig. 2. Induction of the Dex gene signature by DexP liposomes. Primary human monocytes were incubated for 24 h with free Dex and PEG or PS DexP liposomes at a nominal Dex concentration of 1 μg/mL, drug-free PEG or PS liposomes or left without treatment. Expression of a set of genes characteristic for various macrophage polarization states was assessed by qPCR using a customized gene array microfluidic card. Expression levels are presented as the fold change relative to untreated cells and amplitude is color coded. The gene signatures for different treatment types (Dex, IL4 or IFNγ) are indicated in the second column. Macrophages from two donors were assayed and are presented in separate panels. (For interpretation of the references to color in this figure legend, the reader is referred to the Web version of this article.)

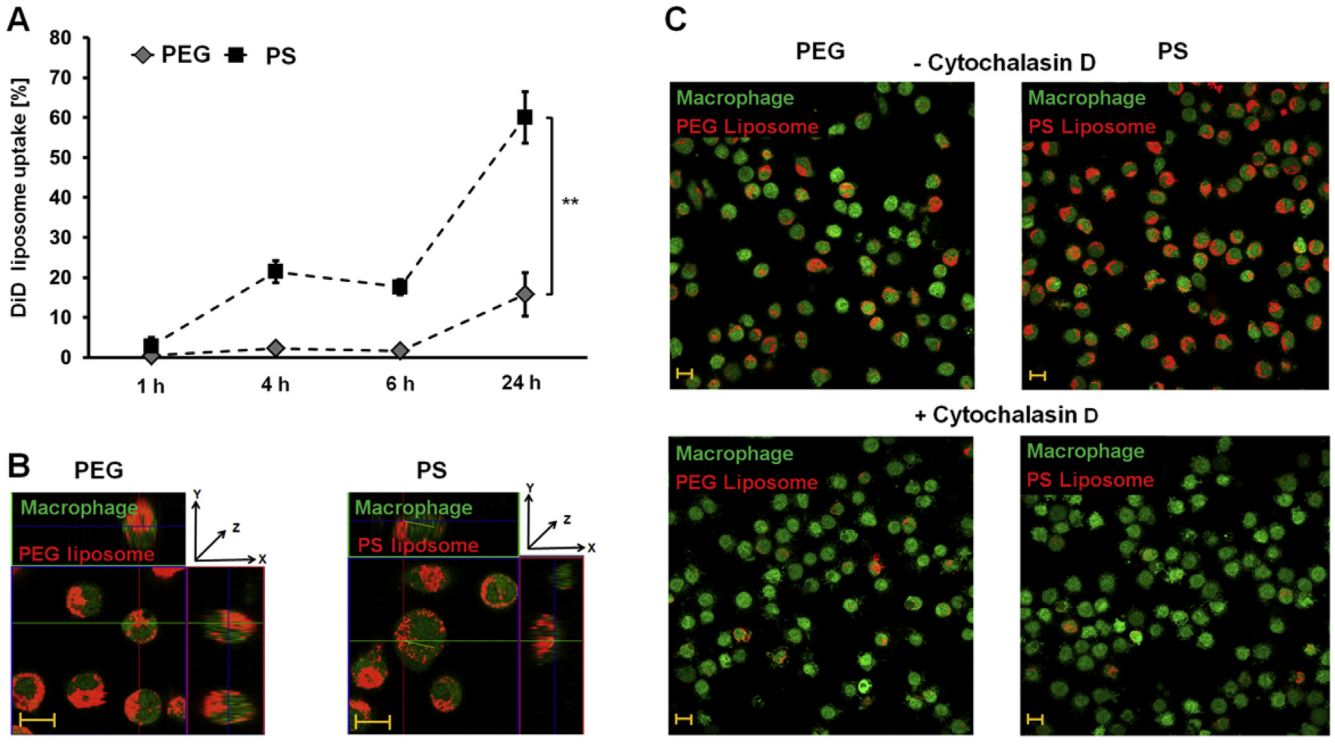

Fig. 3. Kinetics and characterization of DiD-labeled fluorescent liposome uptake. Primary human monocytes were stained with the green fluorescent cell tracker CMFDA and left to attach overnight before treatment with red fluorescent DiD PEG or PS liposomes. (A) Uptake of DiD-labeled liposomes by macrophages was monitored using confocal microscopy imaging at indicated time points (see Supplement Fig. 2 for microscopy images) and quantified as the average % of DiD (red) stained area relative to the macrophage surface area (green) for one single experiment. Comparison between PEG and PS liposomes was carried out using a two-way ANOVA followed by multiple comparisons using Sidak's test with $^{**}P < 0.001$. Error bars indicate the SD for the two to four quantified regions. (B) Z-stacks images from the 24 h time point were taken over 10 planes of approximately 1.7 μm depth each. A representative central z-plane is shown with x-y axis visualization to see liposome internalization for the PEG liposomes (left) and the PS liposomes (right). (C) Liposome uptake was assessed (top) absence or (bottom) presence of co-treatment with cytochalasin D (bottom) at 24 h for two independent experiments; a representative region is shown for each condition. The scale bars indicate 10 μm in all images.

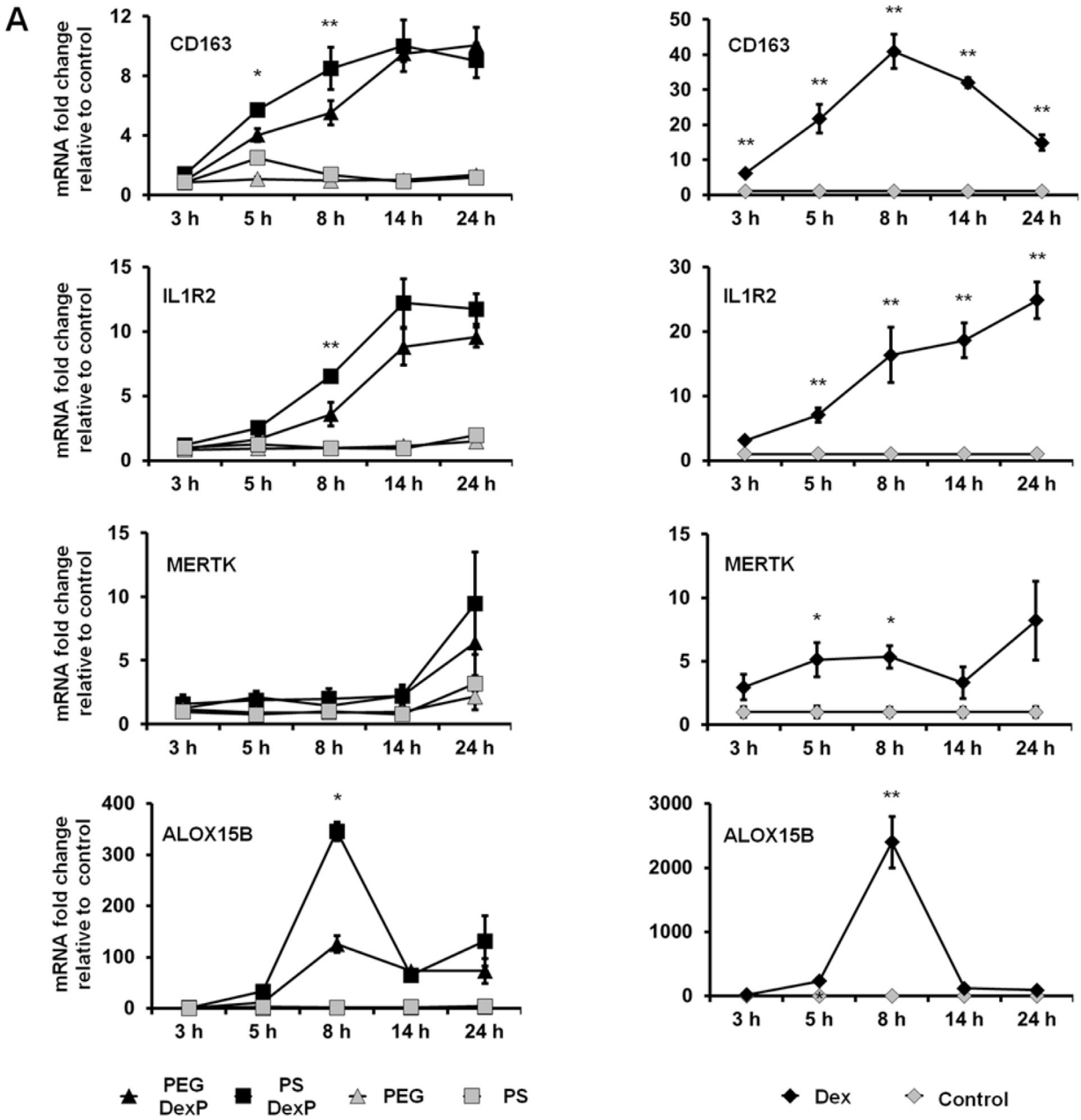
A
CD163
IL1R2
MERTK
ALOX15B
mRNA fold change relative to control
3 h
5 h
8 h
14 h
24 h
PEG DexP
PS DexP
PEG
PS
Dex
Control

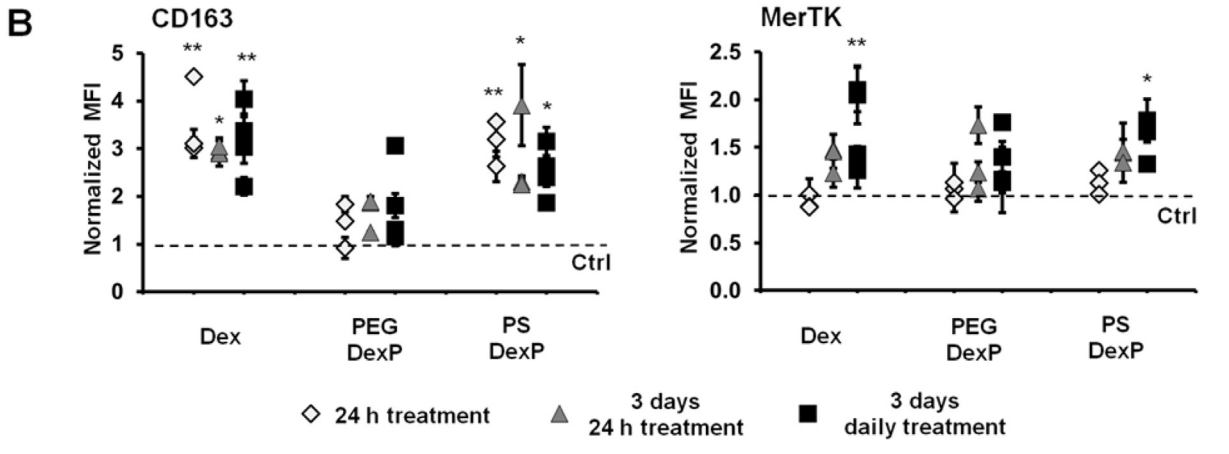
B
CD163
MerTK
Normalized MFI
Ctrl
Dex
PEG DexP
PS DexP
24 h treatment
3 days 24 h treatment
3 days daily treatment

than that of free Dex. The confidence intervals (CIs) for the DexP PEG and PS liposomes were overlapping, indicating that the response of the two formulations could not be differentiated in the present setting (Supplement Fig. 3). At the highest tested concentration, our reference concentration of 1 μg/mL, Dex delivered by liposomes did not reach the maximal efficacy of free Dex. As the maximal transcriptional effect was reached in these conditions and as the decrease of cytokine release is comparatively more sensitive to Dex [35,45], these results suggest some kinetic differences or signaling interference by the liposomes themselves, e.g. as suggested in the studies by Bartneck et al. [45]. Drug-free liposomes had no effect on LPS-induced cytokine levels (Supplement Fig. 3), suggesting that the PS liposomes do not fully mimic the role of apoptotic cells with regard to induction of anti-inflammatory effects in macrophages [47–49].

We also show that the Dex-induced release of the pro-resolutive factor Thrombospondin 1 (TSP1) [50–53] is reproduced by treatment of macrophages with DexP liposomes (Fig. 5B). In macrophages tested from three donors, PS DexP liposomes showed a robust TSP1 increase, similar to the levels reached by free Dex treatment. PEG DexP liposomes exhibited a more variable response. Drug-free PEG and PS liposomes had no effect on TSP1 levels (Supplement Fig. 3). In a tissue repair context, TSP1 release by macrophages may stimulate functions complementary to the decrease of pro-inflammatory cytokines [54], namely the release of IL10 [55,56] and the activation of TGFβ1 [57–61].

3.4. Induction of an anti-inflammatory phenotype in inflammatory macrophages

In order to further characterize the capacity of liposomes to polarize not only infiltrating monocytes but also the established pro-inflammatory macrophages present in inflamed tissue, we performed a pro-to anti-inflammatory phenotype switch experiment. We cultured monocytes for three days in growth medium to generate mature, control macrophages or in medium containing IFNγ to concomitantly drive the macrophages to an inflammatory state. The latter was verified by qPCR, using CXCL11 and CD38, two markers from the IFNγ pro-inflammatory gene signature (selected from the study available at ArrayExpress, E-MTAB-5913) (Fig. 6A).

Treatment of these inflammatory macrophages with free Dex or DexP in liposomes induced an upregulation of Dex-marker genes, as characterized for monocytes, showing that these macrophages also efficiently take up and process DexP liposomes (Fig. 6B). According to this marker gene profile, DexP liposomes are able to drive the inflammatory macrophages to a Dex-like, anti-inflammatory phenotype. Further, as PS DexP liposomes induced a stronger gene signature, their superior efficacy compared to PEG DexP liposomes is further confirmed in this setting. Drug-free liposomes have no major effect on the expression of these genes in inflammatory macrophages, as observed in monocyte cultures.

Mature control and inflammatory macrophages treated with free Dex or DexP liposomes showed a decrease in LPS-induced TNFα and IL6 (Fig. 6C). Free Dex exhibited a similar potency as that seen in monocyte cultures (Fig. 5A and Supplement Fig. 3), with IC50s for TNFα of 4.9 ng/mL on control macrophages and 4.4 ng/mL on pro-inflammatory macrophages. The potency of the DexP liposomes was lower than that of free Dex, however, it is noteworthy that PS liposomes (and not PEG liposomes) show a better efficacy on control or inflammatory macrophages compared to cultured monocytes (Supplement Fig. 3). This likely relates to a higher phagocytic capacity of mature macrophages for molecules with physical properties recapitulated by the PS liposomes. For TNFα, IC50s of 88.9 and 90.1 ng/mL, respectively, were measured for control and inflammatory macrophages with PS DexP liposomes, as compared to 462.7 and 750 ng/mL with PEG DexP liposomes. Consequently, on these mature macrophages, PS DexP liposomes exhibit an activity distinguishable from and more potent than that of PEG DexP liposomes. For IL6, our data led to similar conclusions, with the various treatments inducing overall slightly lower inhibitory responses (Fig. 6C). In particular, it confirmed the better potency of the PS DexP liposomes over the PEG DexP liposomes, with IC50s of 267 ng/mL and >1 ng/mL, respectively, on inflammatory macrophages.

Taken together, we show here that Dex P liposomes can induce an anti-inflammatory phenotype in primary human monocytes as well as in inflammatory macrophages. PS DexP liposomes were overall more effective than PEG DexP liposomes. PS liposomes are known to be better taken up by the mononuclear phagocyte system (MPS) due to their negative charge [62,63], which may explain the better efficacy. The drawback being that they are also quickly removed from the circulation *in vivo* and thus exhibit a short half-life [64]. We therefore consider liposomes for local application and our findings suggest that (PS) liposome-based topical delivery of dexamethasone to macrophages is a promising approach.

We expect PS DexP liposomes to efficiently act on monocytes constantly entering the challenged tissue as well as on the inflammatory macrophages already in place. This should lead to an enhanced *in vivo* efficacy of the proposed delivery system in chronic inflammatory sites such as chronic wounds. In agreement with this notion, Porcheray et al. [65] have shown the importance of the macrophage phenotype switch in the context of resolving inflammation.

3.5. Increase of the efferocytic capacity of DexP liposome-treated macrophages

Efferocytosis is required for the resolution of chronic inflammation and this activity is increased in macrophages upon Dex stimulation. We therefore evaluated the efferocytosis capacity of macrophages treated with DexP liposomes. To this end, we set up an imaging-based phagocytosis assay using CMFDA-labeled macrophages (green) and Cell Trace Violet-labeled apoptotic Jurkat cells (blue). Fas-induced apoptosis of Jurkat cells was monitored for each experiment using FITC-labeled AnnexinV for labeling of externalized PS and an APC-labeled viability dye to track necrotic cells with dysfunctional membranes (Fig. 7A). Phagocytosis and internalization of Jurkat cells in our assay settings was verified by confocal

Fig. 4. Kinetics of gene and protein expression. Primary human monocytes were treated with free Dex and PEG or PS DexP liposomes at a nominal Dex concentration of 1 μg/mL, drug-free PEG or PS liposomes or left without treatment for the indicated time periods. (A) The qPCR expression profiles of the selected genes for the liposome treatments (left panel) and for the free Dex and untreated cells (right panel) are shown as fold change relative to untreated cells (Control). Data represent the mean ± SD for three independent experiments. A two-way ANOVA was performed comparing PS DexP liposomes to PEG DexP liposomes (left panel) and free Dex relative to PEG and PS DexP liposomes (right panel), followed by multiple comparisons using Tukey's test with *P < 0.05; **P < 0.001. (B) Cells were incubated for 24 h with treatment, or for 3 days with treatment for the first 24 h before washing, or for 3 days with daily treatment. Surface protein expression levels from three to four independent experiments were analyzed and quantified by flow cytometry. The mean fluorescence intensity (MFI) values normalized to respective control conditions (i.e. no treatment for free Dex, drug-free liposomes for DexP liposomes) for each independent experiment are shown for CD163 and MerTK. The expression level in untreated cells (Ctrl; dotted line) is given as reference. A two-way ANOVA comparing Dex or DexP liposome treatments to untreated cells was followed by Tukey's multiple comparisons test with *P < 0.05; **P < 0.001. Error bars indicate the range of technical duplicates. Plots for the drug-free liposomes are shown in Supplement Fig. 2.

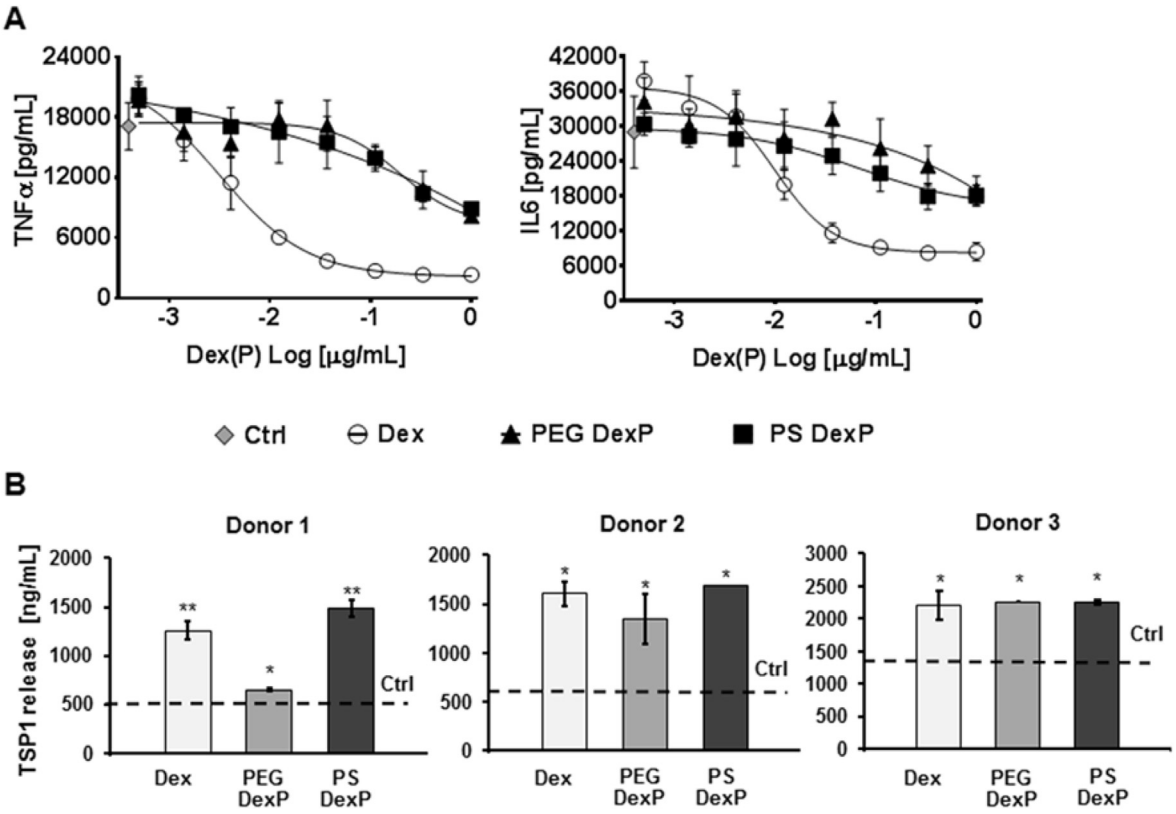

Fig. 5. Secretion of pro-inflammatory and pro-resolutive factors. (A) Primary human monocytes were treated for 24 h with free Dex or DexP liposomes at a nominal concentration of Dex between 0.0005 and 1 µg/mL. LPS-induced TNFα and IL6 release was measured in culture supernatants with an HTRF-based assay and effects of free Dex and DexP liposomes are shown. Data represent the mean ± SD for three independent experiments. (B) TSP1 release was measured in the supernatants of cultures from three independent donors with an ELISA-based assay after treatment with Dex or DexP liposomes at a concentration of 1 µg/mL. The TSP1 level released by untreated cells (Ctrl) is given as reference (dotted line). A one-way ANOVA followed by Tukey's multiple comparisons test compare free Dex and DexP liposome treatments to control cells with $^{*}P < 0.05$; $^{**}P < 0.001$; no significant difference is observed between free Dex and DexP liposomes, except in Donor 1 where TSP1 release is statistically different between free Dex and PEG DexP liposomes. Controls and drug-free liposomes data for (A) and (B) are provided in Supplement Fig. 3.

microscopy (Fig. 7B–C). The principal parameters of the assay being validated, we ran efferocytosis experiments using an automated imaging analysis tool to quantify green (macrophage) and blue (Jurkat) signals and their overlap; multiple areas per condition were analyzed. Quantification of the engulfment of apoptotic cells by macrophages in the various treatment conditions showed that Dex delivery by liposomes increases the efferocytosis to the same extent as free Dex (Fig. 7D). Interestingly, in this setting, PEG DexP liposomes reached an efficacy similar to the one of PS DexP liposomes.

We correlated the efferocytosis levels to the expression of MerTK (Fig. 7E), the membrane receptor well characterized for its functional role in efferocytosis by Dex-polarized macrophages. As expected, the expression of MerTK paralleled the increase in efferocytosis, suggesting it mediated, at least in part, the increased phagocytosis of the apoptotic Jurkat cells. The equivalent membrane level of MerTK in macrophages treated with PEG or PS DexP liposomes (or free Dex) at day 3 suggests that long term treatment allows for maximal Dex efficacy and similar functional potency of the PEG and PS liposomes. Drug-free PEG or PS liposomes failed to increase MerTK expression (confirming Supplement Fig. 2 data) and did not modulate the efferocytosis capacity of macrophages. This assay performed after three days of culture in presence of DexP liposomes shows that long term treatment is important to efficiently deliver Dex to macrophages.

3.6. Preferential uptake of PEG and PS liposomes by monocyte/macrophages in a skin wound environment

Published work supports the central role of macrophages in chronic inflammatory diseases and shows their essential role in tissue repair and wound healing [66–70]. However, literature reports on the use of GC-containing carriers or liposomes in skin wound models are limited. One group showed that macrophage activity and the wound healing process can be influenced by GC-loaded liposomes in an acute model [71]. Indeed, Dex-polarized macrophages represent a desirable phenotype in this respect. Efferocytosis, increased in Dex-treated macrophages, removes debris and clears apoptotic cells before they undergo secondary necrosis. Further, it has been suggested that efferocytosis-primed macrophages secrete pro-resolutive signals (reviewed in Ref. [72]). Above we could show a strong decrease of the pro-inflammatory cytokines IL6 and TNFα, both present in chronic wound fluids, and an increased expression or secretion of the resolutive factors LX15B (ALOX15B gene) and TSP1. Also, the observed robust increase in the expression of the decoy receptor IL1R2 is of interest, as wound fluid is known to contain high levels of IL1β [73,74], a strong pro-inflammatory cytokine that maintains the inflammatory milieu. Hence, Dex-polarized macrophages exhibit characteristics that are appropriate to stop the positive feedback loop maintaining inflammation and to modulate the microenvironment towards homeostasis and reach tissue repair.

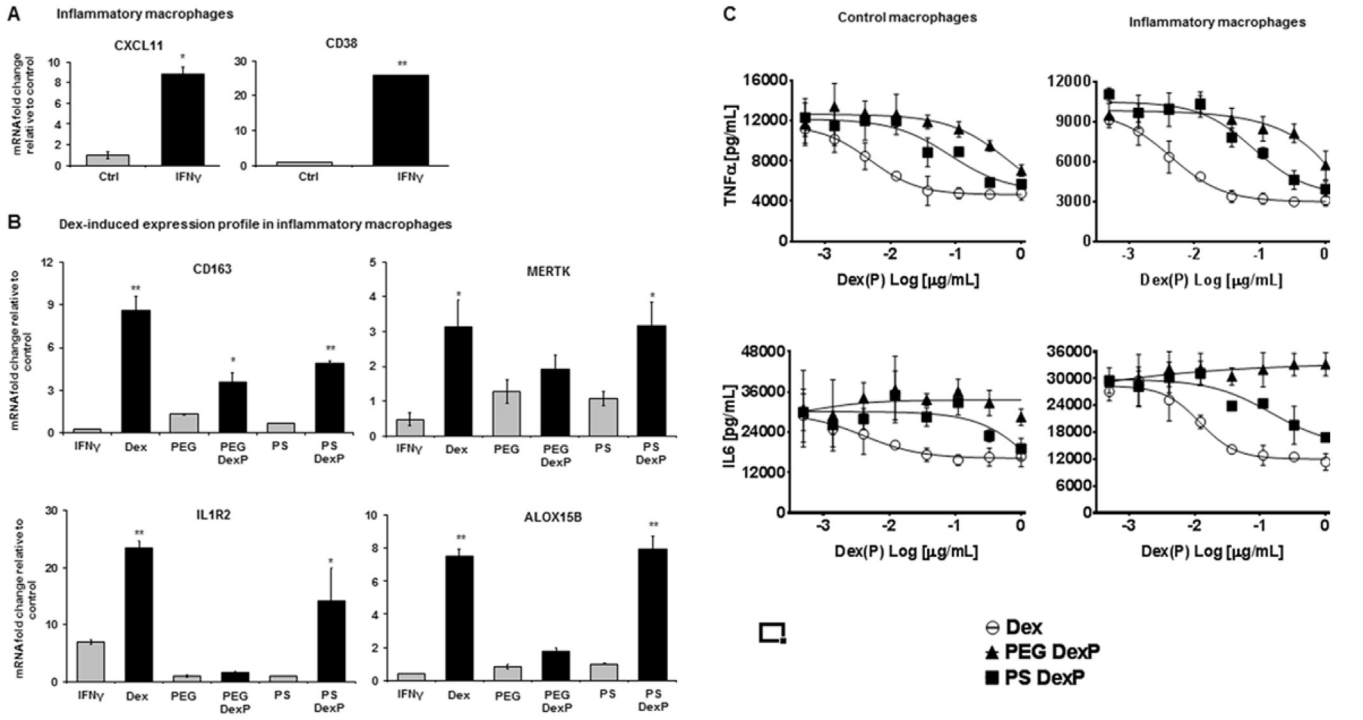

Fig. 6. Phenotype switch in pro-inflammatory macrophages treated with DexP liposomes. (A) Primary human monocytes were grown for 3 days to generate control macrophages or inflammatory macrophages by addition of IFNγ; induction of the inflammatory phenotype is shown by qPCR profiling. (B) IFNγ-induced macrophages were then treated for 24 h with free Dex and PEG or PS DexP liposomes at a nominal Dex concentration of 1 µg/mL, drug-free PEG or PS liposomes or left without further treatment (IFNγ). The qPCR expression profile for the Dex-regulated genes is shown as fold change relative to untreated cells for one representative experiment out of three independent experiments. Error bars represent the SD of technical duplicates. A one-way ANOVA comparing free Dex to IFNγ or DexP liposome to drug-free liposome treatments was performed followed by Tukey's multiple comparisons test with *P < 0.05; **P < 0.001. (C) Control or inflammatory macrophages were treated with a range of concentration of Dex, PEG or PS DexP liposomes or drug-free liposomes. Culture supernatants were analyzed for LPS-induced TNFα and IL6 release using an HTRF-based assay. Data represent the mean ± SD for three independent experiments. Controls with drug-free liposomes are shown in Supplement Fig. 3.

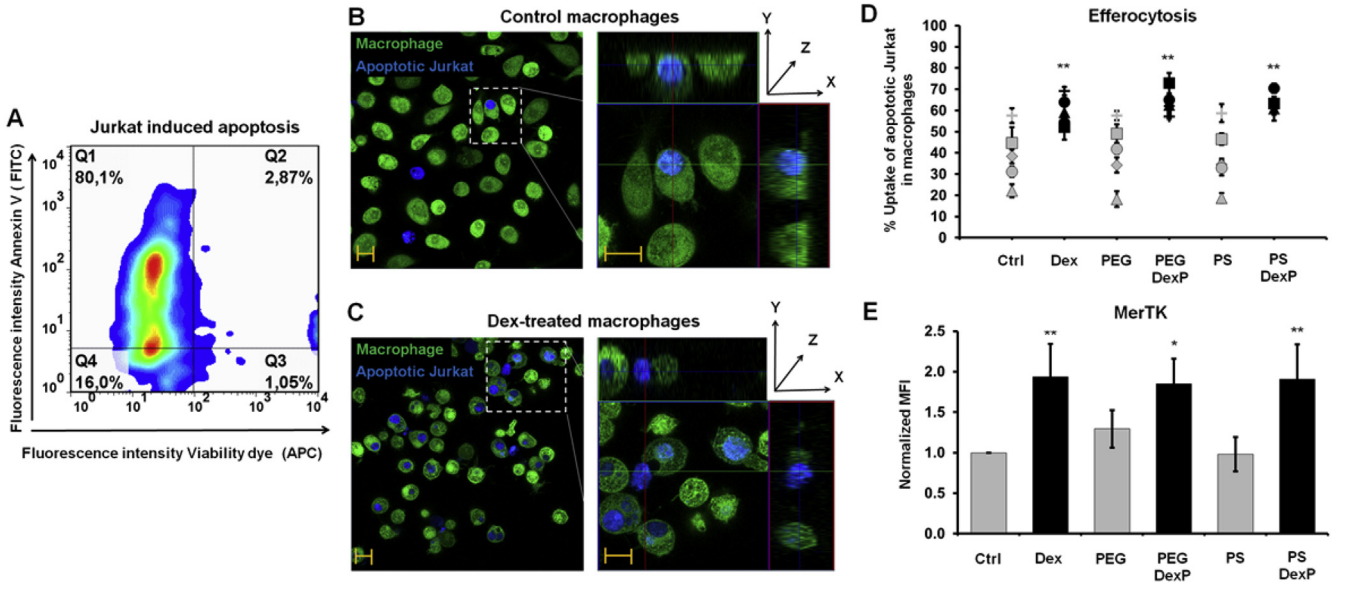

Fig. 7. Efferocytosis and MerTK protein expression. (A) FAS-ligand induced apoptosis of Jurkat cells was verified by flow cytometry by quantifying AnnexinV positive cells and viability dye-negative cells (Q1). Q2 shows late apoptotic cells, Q3 shows dead or necrotic cells and Q4 shows healthy cells. (B–C) Confocal microscopy images of (B) untreated or (C) Dex-treated CMFDA-labeled macrophages (green) engulfing apoptotic Jurkat cells stained with Cell Trace Violet (blue), representative of the images used for quantification of efferocytosis, including a central z-plane with x-y axis visualization highlighting Jurkat cell internalization. The scale bar indicates 10 µm. (D–E) Primary human monocytes were treated daily for 3 days with free Dex and PEG or PS DexP liposomes at a nominal Dex concentration of 1 µg/mL, or with drug-free liposomes or left untreated (Ctrl). (D) Efferocytosis was assessed on the same macrophages as those used for MerTK expression and measured as the percentage of macrophages having phagocytosed apoptotic Jurkat cells over the total number of macrophages. Five independent experiments with macrophages from different donors are shown. Each symbol corresponds to one donor and error bars indicate the SD for technical triplicates. (E) The expression of MerTK was analyzed by flow cytometry and is shown as the MFI values normalized to the untreated (Ctrl) condition. Data represent the mean ± SD for five independent experiments. A one-way ANOVA followed by Tukey's multiple comparison test was used to compare treatments to untreated cells with *P < 0.05; **P < 0.001.

We therefore investigated the specificity of liposome uptake by different cell types in view of applying the DexP liposomes to wounds. In initial experiments we chose to compare uptake by macrophages, keratinocytes and fibroblasts. The latter two cell types are crucial for wound healing and are affected *in vivo* by Dex, mediating GC side effects [75]. Similarly to the uptake experiments described above, we incubated DiD-labeled liposomes with 2D cultures of CMFDA-labeled human dermal fibroblasts or human dermal keratinocytes and evaluated the uptake by confocal microscopy imaging. Uptake and internalization of liposomes into both cell types was observed, similarly for the two formulations as judged by visual inspection (Fig. 8A). Importantly, quantification of the internalized liposomes in keratinocytes and fibroblasts showed much reduced levels as compared to macrophages and there was no robust difference between the two cell types (Fig. 8B). With regard to uptake into macrophages, the present experiments again confirm the advantage of PS over PEG liposomes (compare to Fig. 3).

We next investigated the behavior of the liposome formulations in a more complex environment, a wounded skin equivalent. We established a 3D full thickness skin model based on human primary dermal fibroblasts embedded in a collagen matrix forming the dermal layer and a stratifying human primary epidermal keratinocyte overlay forming the epidermis (Fig. 9A). We then developed a wounded skin equivalent version (Fig. 9B–C) to mimic a skin injury and to allow for testing the fate of locally applied liposomes. We showed that macrophages added into the wound of the skin model rapidly internalized (Dil-labeled) PEG and PS liposomes, within 24 h, as observed in the 2D macrophage cultures (Fig. 9D). The red stains in macrophages was intense, suggesting a strong avidity of macrophages for liposomes and an efficient uptake; representative pictures are shown. On the other hand, stained liposomes were barely detected in cells other than macrophages. In order to better evaluate liposome uptake by keratinocytes and fibroblasts, a protocol with labeled fibroblasts and keratinocytes was established. It allowed for better identification and tracking of these cell types. Addition of liposomes to this model confirmed the very limited uptake of liposomes by keratinocytes and fibroblasts; the pictures shown illustrate rare uptake events in fibroblasts and keratinocytes in the absence of macrophages in the wound bed (Fig. 9E). The almost complete absence of liposome uptake by stratified keratinocytes in the upper cornified layer is not too surprising, similar to what is expected in intact skin. However, it is highly interesting to note that migrating keratinocytes engaged in wound closure did not show liposome uptake (Fig. 9D). Further experiments with co-addition of labeled macrophages and Dil liposomes into wounds confirmed the favored uptake of liposomes by macrophages in a skin wound environment (Supplement Fig. 5). These data suggest that in a chronic wound, where a continuous infiltration of monocytes is maintained by the inflammatory milieu, liposomes delivered to the wound bed would first and preferably be taken up by macrophages.

This observation is a strong argument in favor of the proposed treatment with liposomes as keratinocytes represent the main target cell type for GC toxicity in topical treatments. Hence, in chronic wounds, we expect the wound bed macrophages and the constantly infiltrating monocytes to be polarized, while other cell types should not be affected. Local delivery of DexP liposomes to chronic wounds is therefore expected to promote resolution of inflammation and tissue repair, while preserving surrounding cells from undesired Dex effects. This represents a key aspect, as the macrophages mediate their regenerative role in part by ensuring the proper function of the other wound cell types such as keratinocytes and fibroblasts [76]. Further validation of the proposed approach will include preclinical wound healing models. Classically, db/db mice are used, which represent a delayed healing model [77]. As an interesting alternative, an iron overload-induced animal model has been established that mimicks several aspects of venous leg ulcer condition [78]. *In vivo* studies will allow for a more comprehensive characterization of liposome effects, including potential uptake by other immune cells, such as neutrophils, present in high numbers at inflammation sites. Neutrophils are highly phagocytic cells, especially with regard to opsonized material. Engulfment of GC-loaded DexP liposomes by neutrophils would represent an advantage as GCs are known to decrease transmigration of neutrophils and would thus reduce their recruitment to the wound site [79,80].

Higher efficacy of our delivery platform may be achieved by encapsulating GCs with higher potency; such molecules have been developed, including long acting derivatives [81,82]. Associated with slow release of the liposomes, they may deliver an efficacious

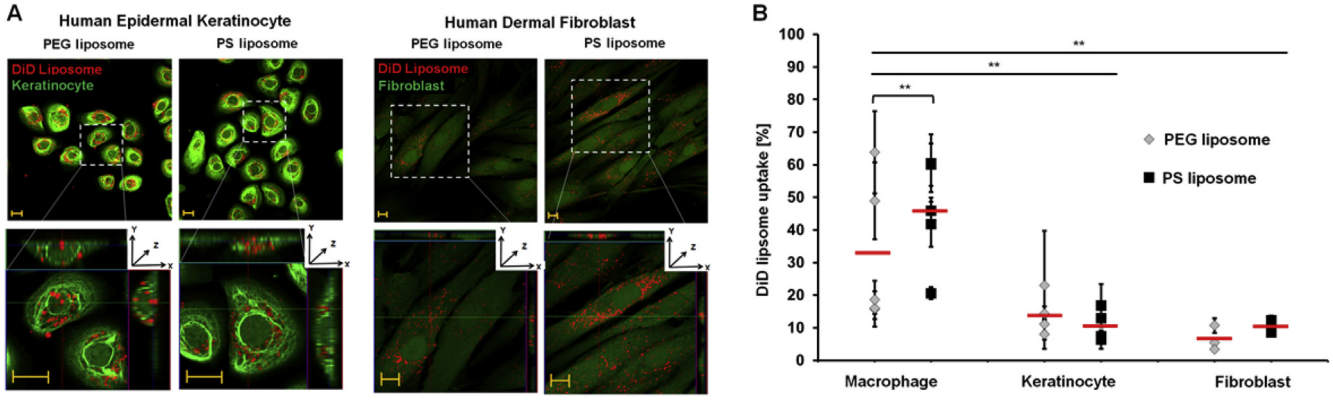

Fig. 8. Fluorescent liposome internalization in keratinocytes and fibroblasts. (A) Primary human fibroblasts or keratinocytes labeled with green fluorescent cell tracker CMFDA were treated with red fluorescent DiD PEG or PS liposomes for 24 h. Confocal microscopy images and stacks were taken over 3–5 z-planes (zoom x1) for fibroblasts and 10–15 z-planes (zoom x2) for keratinocytes of approximately 1.7 μm depth each. Representative images from three and four independent experiments for fibroblasts and keratinocytes, respectively, are shown. A representative central z-plane is shown with x-y axis representation to visualize liposome internalization. The scale bar indicates 10 μm. (B) Uptake was quantified using confocal microscopy images by measuring the % of DiD (red) stained area relative to the macrophage, keratinocyte or fibroblast surface area (green). The average % of uptake is shown for four to six randomly selected regions (SD indicated by error bars). Data of 5, 4 and 3 independent experiments are shown for macrophages, keratinocytes and fibroblasts, respectively, with averages indicated by red horizontal bars. A two-way ANOVA followed by Tukey's multiple comparison was used to compare uptake between cell types and Sidak's multiple comparisons test was used for each cell type to compare the two formulations, with *P < 0.05; **P < 0.001.

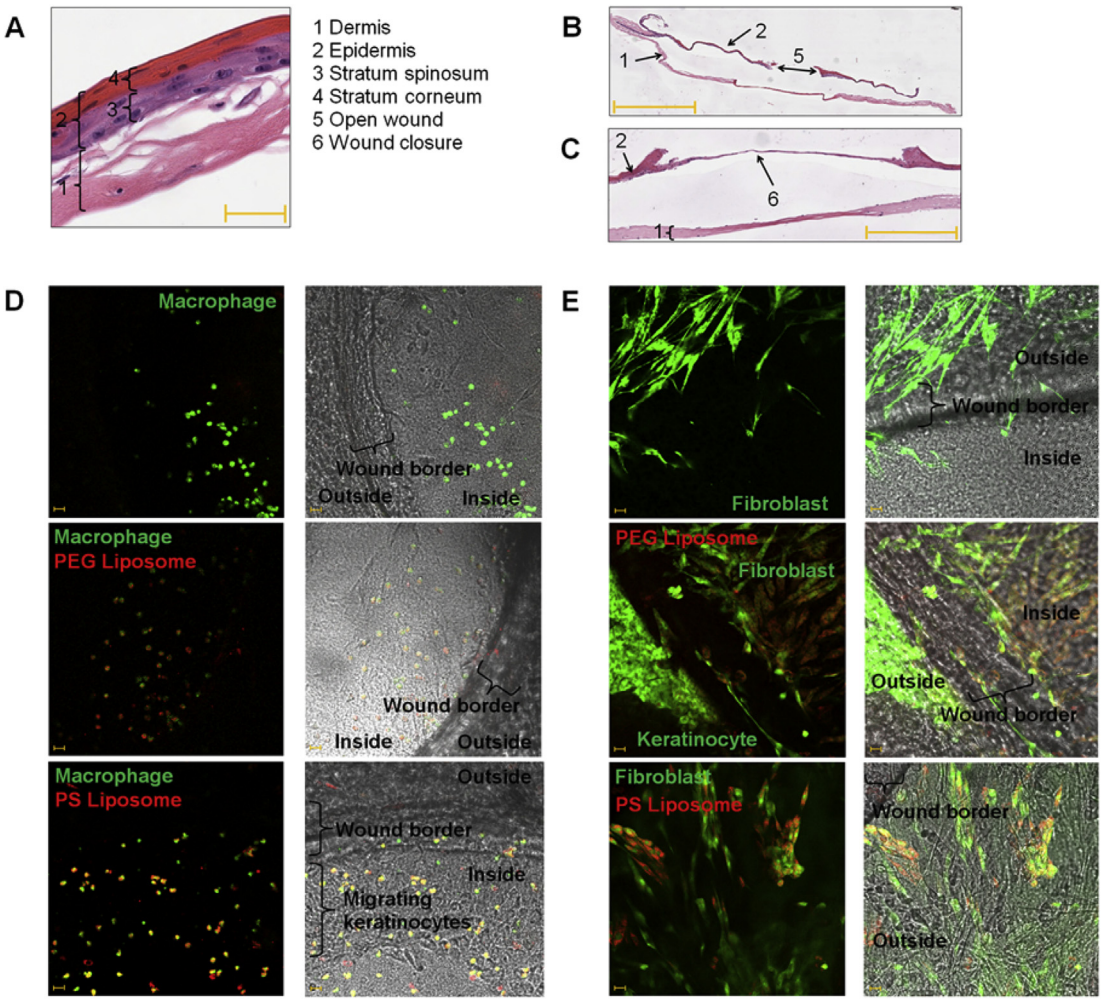

Fig. 9. Distribution and cellular uptake of fluorescent liposomes in a wounded 3D full thickness skin model. Hematoxylin and Eosin staining of paraffin sections of the 3D skin equivalent composed of primary human fibroblasts in collagen and primary human keratinocytes. (A) Intact skin model; the scale bar indicates 100 μm. (B) Wounded skin model; the scale bar indicates 0.1 cm. (C) Wounded model after epithelial wound closure upon keratinocyte migration and proliferation; the scale bar indicates 500 μm. Please note that in (B) and (C), the dermis and epidermis detached from each other during the embedding process due to the fragility of the skin model. (D) CMFDA-stained human primary macrophages (green) and/or DiI-labeled liposomes (red) were added into the wound of the 3D skin construct for 24 h. Images, captured with a two-photon laser scanning confocal microscope, were taken in a region around the wound border and show the wound with macrophages only (top), with macrophages and DiI PEG liposomes (middle) and with macrophages and DiI PS liposomes (bottom). The wound border defines the ring resulting from keratinocyte exclusion caused by plug insertion and subsequent removal (wounded area); the outside area corresponds to dermo-epidermal equivalent; the inside area represents the wound, the dermis equivalent area over which keratinocytes migrate and eventually differentiate to close the wound. The experiment was performed in duplicate. Representative pictures for liposome uptake by macrophages and a selected view of migrating keratinocytes are shown. The scale bar indicates 20 μm. (E) DiI-labeled liposomes were added to the wound of a 3D skin construct for 24 h. The fibroblasts and keratinocytes in the model were stained with calcein green and images were taken with a two-photon laser scanning confocal microscope. Images show areas around the wound border without liposomes (top), with DiI PEG liposomes (middle) and with DiI PS liposomes (bottom). The experiment was performed in technical duplicates. Selected pictures show limited liposome uptake in fibroblasts and keratinocytes in the absence of macrophages. The scale bar indicates 20 μm.

dose over extended time periods and may represent an optimal delivery system. Also, matrices such as hydrogels have already been investigated for sustained delivery of liposome-encapsulated effector molecules. For example, using hydrophilic matrices, Kim and Martin [83] showed release of Dex-loaded nanoparticles over two weeks. Similarly, lipid nanoparticle-based dressings were developed for topical treatment of chronic wounds with growth factors [84]. Such matrices may be useful for validation of the concept in *in vivo* models of chronic wounds.

Other approaches for optimization of our delivery platform may include the development of more potent and more specific liposomes paying particular attention to the inclusion of PS in the membrane [85]. IL6 and TNFα release, but also IL10 and TGFβ, are modulated upon stimulation of macrophages with 'eat me signals' that include PS recognition (reviewed in Ref. [43]). The concept also applies to virus particles that can be considered as 'nanoversions' of PS-displaying apoptotic cells ('apoptotic mimicry') [86]. The PS-containing liposomes used in this work did not fully reproduce the behavior of apoptotic cells (Figs. 2, 4, Supplement Fig. 2-3 and data not shown). It is likely that apoptotic membrane co-factors required for PS recognition are important and the exact quantity of PS as well as the size of the liposomes may represent parameters to be optimized. The study of apoptotic cell-derived microparticles may support the development of liposomes with increased phagocytic potential. For example, addition of membrane proteins providing 'find me' type of signals to the macrophages could prepare them for engulfment and allow higher rates of liposome internalization and more efficient downstream effector functions [20].

4. Conclusion

The central role of macrophages as key modulators able to drive chronic inflammation towards tissue repair is more and more recognized, and macrophages are being increasingly investigated in clinical trials as cellular therapies or targets of innovative drugs. With the present work, we aim to augment the intrinsic potential of macrophages by selectively stimulating them with GCs, effective anti-inflammatory drugs with proven efficacy in several chronic diseases. We demonstrate that the molecular mechanism of action is similar for DexP liposomes and for the free drug, and we show that the liposomes themselves (drug-free) are largely inert in terms of influencing macrophage polarization and function. In addition, we provide first results demonstrating that PS-modified liposomes have advantages over PEG-modified liposomes for local macrophage targeting in the proposed setting of skin wounds. In particular, we show a very limited effect on keratinocytes, the main mediators of GC side effects in the skin. Thus, our data support further investigations for developing a robust liposome-based platform for treating chronic wounds.

Conflicts of interest

AG, AF, KS, BB, HR, AA, MR and MGL are employees of Novartis Pharma AG.

Data availability

The raw/processed data required to reproduce these findings cannot be shared at this time due to technical or time limitations.

Acknowledgements

We gratefully acknowledge support from Bernd Riebesehl, Harry Tiemessen, Patric Baumann and Christiane Schiedel for liposome-related work, Gregory Marszalek, Caterina Safina and Solange Vidal for macrophage-related work and Martin Steinmann for the 2P microscopy. We also thank Susan Kirkland, Gabi Schutzius and Sanaz Afrouznia for support for the keratinocyte-related work. Partial financial support was provided by the German Research Foundation (SFB/TRR57) and the European Research Council (StG-309495-NeoNaNo).

Appendix A. Supplementary data

Supplementary data related to this article can be found at https://doi.org/10.1016/j.biomaterials.2018.04.006.

References

[1] Y.C. Liu, X.B. Zou, Y.F. Chai, Y.M. Yao, Macrophage polarization in inflammatory diseases, Int. J. Biol. Sci. 10 (5) (2014) 520–529.
[2] W. Ohashi, K. Hattori, Y. Hattori, Control of macrophage dynamics as a potential therapeutic approach for clinical disorders involving chronic inflammation, J. Pharmacol. Exp. Therapeut. 354 (3) (2015) 240–250.
[3] J.N. Fullerton, D.W. Gilroy, Resolution of inflammation: a new therapeutic frontier, Nat. Rev. Drug Discov. 15 (8) (2016) 551–567.
[4] A.R. Fraser, C. Pass, P. Burgoyne, A. Atkinson, L. Bailey, A. Laurie, et al., Development, functional characterization and validation of methodology for GMP-compliant manufacture of phagocytic macrophages: a novel cellular therapeutic for liver cirrhosis, Cytotherapy 19 (9) (2017) 1113–1124.
[5] B.A. Mast, G.S. Schultz, Interactions of cytokines, growth factors, and proteases in acute and chronic wounds, Wound Repair Regen. 4 (4) (1996) 411–420.
[6] M.A. Loots, E.N. Lamme, J. Zeegelaar, J.R. Mekkes, J.D. Bos, E. Middelkoop, Differences in cellular infiltrate and extracellular matrix of chronic diabetic and venous ulcers versus acute wounds, J. Invest. Dermatol. 111 (5) (1998) 850–857.
[7] N.B. Menke, K.R. Ward, T.M. Witten, D.G. Bonchev, R.F. Diegelmann, Impaired wound healing, Clin. Dermatol. 25 (1) (2007) 19–25.
[8] T.J. Koh, L.A. DiPietro, Inflammation and wound healing: the role of the macrophage, Exp. Rev. Mol. Med. 13 (2011) e23.
[9] P. Martin, R. Nunan, Cellular and molecular mechanisms of repair in acute and chronic wound healing, Br. J. Dermatol. 173 (2) (2015) 370–378.
[10] N.J. Trengove, H. Bielefeldt-Ohmann, M.C. Stacey, Mitogenic activity and cytokine levels in non-healing and healing chronic leg ulcers, Wound Repair Regen. 8 (1) (2000) 13–25.
[11] R.J. Snyder, J. Lantis, R.S. Kirsner, V. Shah, M. Molyneaux, M.J. Carter, Macrophages: a review of their role in wound healing and their therapeutic use, Wound Repair Regen. 24 (4) (2016) 613–629.
[12] R. Zhao, H. Liang, E. Clarke, C. Jackson, M. Xue, Inflammation in chronic wounds, Int. J. Mol. Sci. 17 (12) (2016).
[13] M. Vaalamo, M. Weckroth, P. Puolakkainen, J. Kere, P. Saarinen, J. Lauharanta, et al., Patterns of matrix metalloproteinase and TIMP-1 expression in chronic and normally healing human cutaneous wounds, Br. J. Dermatol. 135 (1) (1996) 52–59.
[14] R. Blakytny, E. Jude, The molecular biology of chronic wounds and delayed healing in diabetes, Diabet. Med. 23 (6) (2006) 594–608.
[15] O. Stojadinovic, I. Pastar, S. Vukelic, M.G. Mahoney, D. Brennan, A. Krzyzanowska, et al., Deregulation of keratinocyte differentiation and activation: a hallmark of venous ulcers, J. Cell Mol. Med. 12 (6B) (2008) 2675–2690.
[16] N.X. Landen, D. Li, M. Stahle, Transition from inflammation to proliferation: a critical step during wound healing, Cell. Mol. Life Sci. 73 (20) (2016) 3861–3885.
[17] D.W. Cain, J.A. Cidlowski, Specificity and sensitivity of glucocorticoid signaling in health and disease, Best Pract. Res. Clin. Endocrinol. Metabol. 29 (4) (2015) 545–556.
[18] S. Vandevyver, L. Dejager, J. Tuckermann, C. Libert, New insights into the anti-inflammatory mechanisms of glucocorticoids: an emerging role for glucocorticoid-receptor-mediated transactivation, Endocrinology 154 (3) (2013) 993–1007.
[19] A. Ariel, C.N. Serhan, New lives given by cell death: macrophage differentiation following their encounter with apoptotic leukocytes during the resolution of inflammation, Front. Immunol. 3 (2012) 4.
[20] I.K. Poon, C.D. Lucas, A.G. Rossi, K.S. Ravichandran, Apoptotic cell clearance: basic biology and therapeutic potential, Nat. Rev. Immunol. 14 (3) (2014) 166–180.
[21] J. Ehrchen, L. Steinmuller, K. Barczyk, K. Tenbrock, W. Nacken, M. Eisenacher, et al., Glucocorticoids induce differentiation of a specifically activated, anti-inflammatory subtype of human monocytes, Blood 109 (3) (2007) 1265–1274.
[22] G. Zahuczky, E. Kristof, G. Majai, L. Fesus, Differentiation and glucocorticoid regulated apopto-phagocytic gene expression patterns in human macrophages. Role of Mertk in enhanced phagocytosis, PLoS One 6 (6) (2011), e21349.
[23] G. Zizzo, B.A. Hilliard, M. Monestier, P.L. Cohen, Efficient clearance of early apoptotic cells by human macrophages requires M2c polarization and MerTK induction, J. Immunol. 189 (7) (2012) 3508–3520.
[24] V.A. Fadok, D.L. Bratton, A. Konowal, P.W. Freed, J.Y. Westcott, P.M. Henson, Macrophages that have ingested apoptotic cells *in vitro* inhibit proinflammatory cytokine production through autocrine/paracrine mechanisms involving TGF-beta, PGE2, and PAF, J. Clin. Invest. 101 (4) (1998) 890–898.
[25] M.-L.N. Huynh, V.A. Fadok, P.M. Henson, Phosphatidylserine-dependent ingestion of apoptotic cells promotes TGF-β1 secretion and the resolution of inflammation, J. Clin. Invest. 109 (1) (2002) 41–50.
[26] M. Lucas, L.M. Stuart, J. Savill, A. Lacy-Hulbert, Apoptotic cells and innate immune stimuli combine to regulate macrophage cytokine secretion, J. Immunol. 171 (5) (2003) 2610–2615.
[27] M.P. Motwani, D.W. Gilroy, Macrophage development and polarization in chronic inflammation, Semin. Immunol. 27 (4) (2015) 257–266.
[28] R.E. Voll, M. Herrmann, E.A. Roth, C. Stach, J.R. Kalden, I. Girkontaite, Immunosuppressive effects of apoptotic cells, Nature 390 (6658) (1997) 350–351.
[29] C. Wicke, B. Halliday, D. Allen, N.S. Roche, H. Scheuenstuhl, M.M. Spencer, et al., Effects of steroids and retinoids on wound healing, Arch. Surg. 135 (11) (2000) 1265–1270.
[30] H.D. Beer, R. Fassler, S. Werner, Glucocorticoid-regulated gene expression during cutaneous wound repair, Vitam. Horm. 59 (2000) 217–239.
[31] H. Schäcke, W.-D. Döcke, K. Asadullah, Mechanisms involved in the side effects of glucocorticoids, Pharmacol. Therapeut. 96 (1) (2002) 23–43.
[32] S. Schoepe, H. Schacke, E. May, K. Asadullah, Glucocorticoid therapy-induced skin atrophy, Exp. Dermatol. 15 (6) (2006) 406–420.
[33] L. Kolbe, A.M. Kligman, V. Schreiner, T. Stoudemayer, Corticosteroid-induced atrophy and barrier impairment measured by non-invasive methods in human skin, Skin Res. Technol. 7 (2) (2001) 73–77.
[34] S. Schoepe, H. Schacke, K. Asadullah, Test systems for the determination of glucocorticoid receptor ligand induced skin atrophy, Dermatoendocrinol 3 (3) (2011) 175–179.
[35] Y. Abraham, B. Gerrits, M.G. Ludwig, M. Rebhan, Gubser keller C. Exploring glucocorticoid receptor agonists mechanism of action through mass cytometry and radial visualizations, Cytometry B Clin Cytom. 92 (1) (2017) 42–56.
[36] M.L. Immordino, F. Dosio, L. Cattel, Stealth liposomes: review of the basic science, rationale, and clinical applications, existing and potential, Int. J. Nanomed. 1 (3) (2006) 297–315.
[37] J.M. Metselaar, M.H. Wauben, J.P. Wagenaar-Hilbers, O.C. Boerman, G. Storm,

Complete remission of experimental arthritis by joint targeting of glucocorticoids with long-circulating liposomes, Arthritis Rheum. 48 (7) (2003) 2059–2066.
[38] B.J. Crielaard, T. Lammers, R.M. Schiffelers, G. Storm, Drug targeting systems for inflammatory disease: one for all, all for one, J. Contr. Release 161 (2) (2012) 225–234.
[39] B. Ozbakir, B.J. Crielaard, J.M. Metselaar, G. Storm, T. Lammers, Liposomal corticosteroids for the treatment of inflammatory disorders and cancer, J. Contr. Release 190 (2014) 624–636.
[40] M. Bartneck, K.M. Scheyda, K.T. Warzecha, L.Y. Rizzo, K. Hittatiya, T. Luedde, et al., Fluorescent cell-traceable dexamethasone-loaded liposomes for the treatment of inflammatory liver diseases, Biomaterials 37 (2015) 367–382.
[41] M. Yang, X. Feng, J. Ding, F. Chang, X. Chen, Nanotherapeutics relieve rheumatoid arthritis, J. Contr. Release 252 (2017) 108–124.
[42] J.E. Vance, G. Tasseva, Formation and function of phosphatidylserine and phosphatidylethanolamine in mammalian cells, Biochim. Biophys. Acta 1831 (3) (2013) 543–554.
[43] M.R. Elliott, K.M. Koster, P.S. Murphy, Efferocytosis signaling in the regulation of macrophage inflammatory responses, J. Immunol. 198 (4) (2017) 1387–1394.
[44] E. Surdziel, I. Clay, F. Nigsch, A. Thiemeyer, C. Allard, G. Hoffman, et al., Multidimensional pooled shRNA screens in human THP-1 cells identify candidate modulators of macrophage polarization, PLoS One 12 (8) (2017), e0183679.
[45] M. Bartneck, F.M. Peters, K.T. Warzecha, M. Bienert, L. van Bloois, C. Trautwein, et al., Liposomal encapsulation of dexamethasone modulates cytotoxicity, inflammatory cytokine response, and migratory properties of primary human macrophages, Nanomedicine 10 (6) (2014) 1209–1220.
[46] Ritter M1, C. Buechler, T. Langmann, E. Orso, J. Klucken, G. Schmitz, The scavenger receptor CD163: regulation, promoter structure and genomic organization, Pathobiology 67 (5–6) (1999) 257–261.
[47] G.C. Ramos, D. Fernandes, C.T. Charao, D.G. Souza, M.M. Teixeira, J. Assreuy, Apoptotic mimicry: phosphatidylserine liposomes reduce inflammation through activation of peroxisome proliferator-activated receptors (PPARs) *in vivo*, Br. J. Pharmacol. 151 (6) (2007) 844–850.
[48] T. Harel-Adar, T. Ben Mordechai, Y. Amsalem, M.S. Feinberg, J. Leor, S. Cohen, Modulation of cardiac macrophages by phosphatidylserine-presenting liposomes improves infarct repair, Proc. Natl. Acad. Sci. U. S. A. 108 (5) (2011) 1827–1832.
[49] M.Z. Hosain, T. Mori, A. Kishimura, Y. Katayama, Synergy between phenotypic modulation and ROS neutralization in reduction of inflammatory response of hypoxic microglia by using phosphatidylserine and antioxidant containing liposomes, J. Biomater. Sci. Polym. Ed. 27 (3) (2016) 290–302.
[50] A. Agah, T.R. Kyriakides, J. Lawler, P. Bornstein, The lack of thrombospondin-1 (TSP1) dictates the course of wound healing in double-TSP1/TSP2-null mice, Am. J. Pathol. 161 (3) (2002) 831–839.
[51] C. Flügel-Koch, A. Ohlmann, R. Fuchshofer, U. Welge-Lüssen, E.R. Tamm, Thrombospondin-1 in the trabecular meshwork: localization in normal and glaucomatous eyes, and induction by TGF-β1 and dexamethasone *in vitro*, Exp. Eye Res. 79 (5) (2004) 649–663.
[52] J.T. Blanco-Mezquita, A.E.K. Hutcheon, J.D. Zieske, Role of Thrombospondin-1 in repair of penetrating corneal WoundsRepair of penetrating corneal wounds, Invest. Ophthalmol. Vis. Sci. 54 (9) (2013) 6262–6268.
[53] F.O. Martinez, S. Gordon, The M1 and M2 paradigm of macrophage activation: time for reassessment, F1000Prime Rep. 6 (2014) 13.
[54] Z. Lopez-Dee, K. Pidcock, L.S. Gutierrez, Thrombospondin-1: multiple paths to inflammation, Mediat. Inflamm. 2011 (2011) 296069.
[55] Y. Zhao, Z. Xiong, E.J. Lechner, P.A. Klenotic, B.J. Hamburg, M. Hulver, et al., Thrombospondin-1 triggers macrophage IL10 production and promotes resolution of experimental lung injury, Mucosal Immunol. 7 (2) (2014) 440–448.
[56] A. King, S. Balaji, L.D. Le, T.M. Crombleholme, S.G. Keswani, Regenerative wound healing: the role of Interleukin-10, Adv. Wound Care 3 (4) (2014) 315–323.
[57] S. O'Kane, M.W. Ferguson, Transforming growth factor beta s and wound healing, Int. J. Biochem. Cell Biol. 29 (1) (1997) 63–78.
[58] S.E. Crawford, V. Stellmach, J.E. Murphy-Ullrich, S.M.F. Ribeiro, J. Lawler, R.O. Hynes, et al., Thrombospondin-1 is a major activator of TGF-β1 *in vivo*, Cell 93 (7) (1998) 1159–1170.
[59] J.E. Nor, L. Dipietro, J.E. Murphy-Ullrich, R.O. Hynes, J. Lawler, P.J. Polverini, Activation of latent TGF-beta1 by thrombospondin-1 is a major component of wound repair, Oral Biosci. Med. OBM 2 (2) (2005) 153–161.
[60] T.A. Wynn, K.M. Vannella, Macrophages in tissue repair, regeneration, and fibrosis, Immunity 44 (3) (2016) 450–462.
[61] A. Kelly, S.A. Houston, E. Sherwood, J. Casulli, M.A. Travis, Regulation of innate and adaptive immunity by TGFbeta, Adv. Immunol. 134 (2017) 137–233.
[62] A. Gabizon, D. Papahadjopoulos, The role of surface charge and hydrophilic groups on liposome clearance *in vivo*, Biochim. Biophys. Acta 1103 (1) (1992) 94–100.
[63] O.C. Boerman, W.J. Oyen, L. van Bloois, E.B. Koenders, J.W. van der Meer, F.H. Corstens, et al., Optimization of technetium-99m-labeled PEG liposomes to image focal infection: effects of particle size and circulation time, J. Nucl. Med. 38 (3) (1997) 489–493.
[64] T.M. Huong, T. Ishida, H. Harashima, H. Kiwada, The complement system enhances the clearance of phosphatidylserine (PS)-liposomes in rat and Guinea pig, Int. J. Pharm. 215 (1–2) (2001) 197–205.
[65] F. Porcheray, S. Viaud, A.C. Rimaniol, C. Leone, B. Samah, N. Dereuddre-Bosquet, et al., Macrophage activation switching: an asset for the resolution of inflammation, Clin. Exp. Immunol. 142 (3) (2005) 481–489.
[66] B.N. Brown, B.M. Sicari, S.F. Badylak, Rethinking regenerative medicine: a macrophage-centered approach, Front. Immunol. 5 (2014) 510.
[67] J.W. Godwin, A.R. Pinto, N.A. Rosenthal, Macrophages are required for adult salamander limb regeneration, Proc. Natl. Acad. Sci. U.S.A. 110 (23) (2013) 9415–9420.
[68] R.E. Mirza, M.M. Fang, W.J. Ennis, T.J. Koh, Blocking interleukin-1beta induces a healing-associated wound macrophage phenotype and improves healing in type 2 diabetes, Diabetes 62 (7) (2013) 2579–2587.
[69] Y. Tang, M.J. Zhang, J. Hellmann, M. Kosuri, A. Bhatnagar, M. Spite, Proresolution therapy for the treatment of delayed healing of diabetic wounds, Diabetes 62 (2) (2013) 618–627.
[70] O. Krenkel, F. Tacke, Liver macrophages in tissue homeostasis and disease, Nat. Rev. Immunol. 17 (5) (2017) 306–321.
[71] C.D. Richters, N.J. Paauw, I. Mayen, L. van Bloois, J.M. Metselaer, G. Storm, J.S. du Pont, M.J. Hoekstra, R.W. Kreis, E.W. Kamperdijk, Administration of prednisolone phosphate-liposomes reduces wound contraction in a rat partial-thickness wound model, Wound Repair Regen. 14 (5) (2006) 602–607.
[72] S. Schif-Zuck, N. Gross, S. Assi, R. Rostoker, C.N. Serhan, A. Ariel, Saturated-efferocytosis generates pro-resolving CD11b low macrophages: modulation by resolvins and glucocorticoids, Eur. J. Immunol. 41 (2) (2011) 366–379.
[73] B.S. Pukstad, L. Ryan, T.H. Flo, J. Stenvik, R. Moseley, K. Harding, et al., Non-healing is associated with persistent stimulation of the innate immune response in chronic venous leg ulcers, J. Dermatol. Sci. 59 (2) (2010) 115–122.
[74] C. Wiegand, U. Schonfelder, M. Abel, P. Ruth, M. Kaatz, U.C. Hipler, Protease and pro-inflammatory cytokine concentrations are elevated in chronic compared to acute wounds and can be modulated by collagen type I *in vitro*, Arch. Dermatol. Res. 302 (6) (2010) 419–428.
[75] A. Sanchis, L. Alba, V. Latorre, L.M. Sevilla, P. Pérez, Keratinocyte-targeted overexpression of the glucocorticoid receptor delays cutaneous wound healing, PLoS One 7 (1) (2012), e29701.
[76] M.P. Rodero, K. Khosrotehrani, Skin wound healing modulation by macrophages, Int. J. Clin. Exp. Pathol. 3 (7) (2010) 643–653.
[77] J. Michaels, S.S. Churgin, K.M. Blechman, M.R. Greives, S. Aarabi, R.D. Galiano, G.C. Gurtner, Db/db mice exhibit severe wound-healing impairments compared with other murine diabetic strains in a silicone-splinted excisional wound model, Wound Repair Regen. 15 (5) (2007) 665–670.
[78] A. Sindrilaru, T. Peters, S. Wieschalka, C. Baican, A. Baican, H. Peter, et al., An unrestrained proinflammatory M1 macrophage population induced by iron impairs wound healing in humans and mice, J. Clin. Invest. 121 (3) (2011) 985–997.
[79] N.J. Goulding, H.S. Euzger, S.K. Butt, M. Perretti, Novel pathways for glucocorticoid effects on neutrophils in chronic inflammation, Inflamm. Res. 47 (3) (1998) S158–S165.
[80] P.S. Weber, T. Toelboell, L.C. Chang, J.D. Tirrell, P.M. Saama, G.W. Smith, J.L. Burton, Mechanisms of glucocorticoid-induced down-regulation of neutrophil L-selectin in cattle: evidence for effects at the gene-expression level and primarily on blood neutrophils, J. Leukoc. Biol. 75 (5) (2004) 815–827.
[81] D.A. Sandham, L. Barker, D. Beattie, D. Beer, L. Bidlake, D. Bentley, et al., Synthesis and biological properties of novel glucocorticoid androstene C-17 furoate esters, Bioorg. Med. Chem. 12 (19) (2004) 5213–5224.
[82] A. Valotis, K. Neukam, O. Elert, P. Högger, Human receptor kinetics, tissue binding affinity, and stability of mometasone furoate, J. Pharmaceut. Sci. 93 (5) (2004) 1337–1350.
[83] D.H. Kim, D.C. Martin, Sustained release of dexamethasone from hydrophilic matrices using PLGA nanoparticles for neural drug delivery, Biomaterials 27 (15) (2006) 3031–3037.
[84] G. Gainza, W.S. Chu, R.H. Guy, J.L. Pedraz, R.M. Hernandez, B. Delgado-Charro, et al., Development and *in vitro* evaluation of lipid nanoparticle-based dressings for topical treatment of chronic wounds, Int. J. Pharm. 490 (1–2) (2015) 404–411.
[85] V. Bagalkot, J.A. Deiuliis, S. Rajagopalan, A. Maiseyeu, Eat me" imaging and therapy, Adv. Drug Deliv. Rev. 99 (Pt A) (2016) 2–11.
[86] J. Mercer, A. Helenius, Vaccinia virus uses macropinocytosis and apoptotic mimicry to enter host cells, Science 320 (5875) (2008) 531–535.